International
Progress Report

IPR-99-14

Äspö Hard Rock Laboratory

First TRUE Stage pilot resin experiment

Pore space analysis

Eva Hakami
Itasca Geomekanik AB, Stockholm

John Gale
Fracflow Consultants Inc., St. John's, Canada

July 1999

Svensk Kärnbränslehantering AB
Swedish Nuclear Fuel
and Waste Management Co
Box 5864
SE-102 40 Stockholm Sweden
Tel 08-459 84 00
+46 8 459 84 00
Fax 08-661 57 19
+46 8 661 57 19

Äspö Hard Rock
Laboratory

Äspö Hard Rock Laboratory

First TRUE Stage pilot resin experiment

Pore space analysis

Eva Hakami
Itasca Geomekanik AB, Stockholm

John Gale
Fracflow Consultants Inc., St. John's, Canada

December 1998

Keywords: TRUE, Resin injection, Fracture sampling, Pore space, Image analysis, Aperture measurement, Variogram analysis, Aperture spatial distribution

This report concerns a study which was conducted for SKB. The conclusions and viewpoints presented in the report are those of the author(s) and do not necessarily coincide with those of the client.

Abstract

The Pilot Resin Experiment Äspö HRL involves the test of epoxy resin behaviour and penetration in fracture planes that are located within a few metres from the drift wall. Samples of two different resin impregnated fracture planes, Samples 1b and 3b, were collected and sectioned perpendicular to the mean fracture plane. A series of sections were cut through the fracture planes and the thickness of the resin filled fracture pore space, the voids, and contact areas were mapped using both a photo-microscope technique and an image analysis technique. The resulting fracture pore space geometry data were analyzed, semi-variograms constructed and the aperture field mapped by kriging. The goal of this study was to compare the relative precision and merits of the two fracture pore space measurement techniques and to analyze and characterize the fracture pore space geometry. The two fracture samples are taken from two fractures with different orientation and different character in terms of geological history and hydromechanical properties. Both fractures are representative of fractures observed at the Äspö HRL.

Both techniques give the same magnitude of aperture, and similar standard deviations. Mean aperture of Sample 1b is about 281 μm. The standard deviation of the aperture is about 37% of the mean aperture. Sample 1b has very little contact area, only about 1% of the whole sample. Mean aperture of Sample 3b is about 295 μm (contact areas and void areas not included). The standard deviation of the aperture is about 39% of the mean aperture. Sample 3b contains about 22% contact area and about 20 % void area.

The photo-microscope technique results in more routine and hence faster processing. The time needed for the image analysis technique is dependent on the particular image contrast conditions of a specific fracture sample. Both measurement techniques would be improved with increased colour contrast between the epoxy resin and the natural materials. In the photo-microscope approach, the photographs and negatives provide a permanent record of the fracture section. Similarly, in the image analysis technique the digital images can be saved and used for additional geometrical or geological analysis or illustrations.

The range of the semi-variogram for the apertures of Sample 1b was determined to about 3.5 mm and to about 5 mm for Sample 3b. This type of spatial distribution data will be important when constructing the conceptual models of the pore space geometry needed in flow and transport modeling. Mapping the aperture field using kriging, based on measurements of apertures and contacts, provides a realistic illustration of the spatial structure, if the measurements are sufficiently densely spaced.

Both of the aperture measurement techniques provide similar results with a similar level of precision for the scale being used. The decision as to which approach to use depends in part on the goal of the aperture measurement exercise. It is recommended that a suitable dye or additive to the resin is identified to facilitate and further increase the quality of the measurements.

Contents

List of Figures

List of Tables

1 Introduction

1.1 Background

In-situ flow and tracer experiments have been conducted in natural fractures at the Äspö Hard Rock Laboratory. One of the key elements required, to fully understand and interpret the results of these flow and tracer experiments, is the pore volume of the tested fractures. Therefore it is important to develop methodologies and techniques to measure the distribution of fracture apertures and characterize the fracture pore volume inside fractures where flow and tracer experiments have been conducted.

A pilot resin injection experiment was carried out, within the framework of the research project TRUE (Tracer Retention Understanding Experiment), where one of the objectives was to develop techniques to be applied during later experimental stages of the TRUE (Winberg, 1999). Resin was injected in fractures at the Pilot Resin site and three 200 mm diameter and three 146 mm diameter drill cores of the resin impregnated fractures have been collected (Birgersson et al., 1999). Parts of the 200 mm cores were selected to be used to compare and evaluate different measurement techniques for assessing aperture (pore volume).

This report contains a presentation of the work carried out by Fracflow Consultants Inc. and Itasca Geomekanik AB. The following sections provide: (1) a summary of the investigative procedures used, (2) a presentation and summary of the data collected, and (3) discussion and recommendations for future investigations.

1.2 Scope and Objectives

The objective of this study was to perform measurements, that can be used to describe the aperture distribution of a selected fracture, and characterize the fracture pore space for *in-situ* fracture conditions.

The objective was also to perform a comparison between data, from measurements using the two slightly different techniques, in order to demonstrate the reliability of aperture measurement data. In addition, the objective was to evaluate the possibilities for development and improvement of the pore volume characterization methods, for future applications in the TRUE project

Two techniques, 1) an image analysis system developed by Royal Institute of Technology, Stockholm (KTH) and 2) a photo-microscope technique developed by Fracflow Consultants Inc., have been applied to measure the fracture apertures in the resin filled fractures. The two techniques used are quite similar in principle. They both

imply measurement of fracture resin layer thickness in sections of drill core samples. The difference is that the "photo-microscope" technique is based on continuous traces (manual digitizing) of the fracture surface profiles and the "image analysis" technique is based on individual measurements, at a chosen separation, in continuous digital images along the profile (the names are not very relevant for the distinction since both approaches use a microscope and image analysis).

2 Measurement Methods

2.1 Sample Preparation

Three sections from the drill cores taken at the Pilot Resin site at Äspö were cut in Oskarshamn and then sent to KTH (see descriptions in Table 1-1). The "Samples" in Table 1-1 are sections of the three 200 mm cores that were expected to contain resin filled fractures. During the core mapping, there seemed to be more resin inside fractures in the 200 mm cores as compared to the 146 mm cores, and therefore samples from the 200 mm cores were chosen for the measurements (Birgersson et al., 1999).

To keep samples intact during cutting, the drillcores were covered with plastic tubes/sleeves and the locations for the cuts were marked on the outer surface of the plastic tubes. The surfaces of the cores and the fracture traces were, however, mapped on transparent plastic before the plastic sleeves were attached. Some of the fractures in the cores were also separated during drilling or core recovery and these fracture planes were glued back together after recovery using a clear epoxy resin. The initial cuts through the drill core were made perpendicular to the core axis. Before making the cuts a reference line from the core mapping was marked along the core.

Prior to further cutting, a thin layer (2 to 3 mm thick and extending about 10 to 15 mm on either side of the fracture plane) of structural epoxy (3M EPX DP 490) was placed over the fracture trace. This epoxy formed a strong bond and reduced the risk of sample separation during sample preparation. Once the epoxy had set, the samples were cut parallel to the fracture plane, using cuts from both sides. The resulting slabs, with the fracture plane in the middle of the slab, are about 50 -70 mm thick (Figure 2-1a).

In order to locate future saw cuts, an arbitrary reference grid was placed on one side of the slabs (Figure 2-1b). One axis of the grid was oriented parallel to the major axis of the ellipse formed by the intersection of the fracture plane and the core surface. The fracture slab was cut twice, perpendicular to the plane of the fracture, producing four quadrants (Figure 2-1b). At this point, about 10 mm thick sections were cut from each quadrant (10 mm including the thickness of the cut itself which is about 2 mm). Before each cut was made on the quadrants, in the perpendicular direction, structural epoxy was applied on the exposed surfaces. The fresh side of each cross-section sawcut was, if needed, grounded slightly to produce a smooth surface for photographing or imaging. Each cross-section was located with a +/- 0.5 mm accuracy to the arbitrary reference grid on the surface of the slab.

Each profile was labeled with reference to the sample name, quadrant, orientation of the profile and its profile number. For example, profile 1bIVX01 represents the first profile (i.e. 01) in the X direction (i.e. X) from Quadrant 4 (i.e. IV) of Sample 1b.

Table 1-1 Location and description, from the drill core mapping of the 200 mm drill cores sections (gray) that were used in this study. Samples marked * contain a fracture which has been glued back together after separation during the sampling.

Sample	Position in borehole, m	Fracture description, resin observations, etc.
KXTE1.a	2.12 - 2.30	Contains intact fracture. Small angle with core axis. Red/Violet resin or dye?
KXTE1.b	2.30 - 2.52	Continuation of fracture in (a).
KXTE1.c	2.53 - 2.83	Continuation of fracture in (a). Also contains another fracture which has been glued together. Red/violet resin on 80%. This fracture has an angle of about 45 degrees with respect to the core axis. (core break)
KXTE2.a	1.50 - 1.65	Contains intact fractures (might be small since they are not seen around the core).
KXTE2.b	1.65 - 1.75	-"-
KXTE2.c *	1.75 - 1.95	Contains fracture which is glued back together. Small angle against core axis. Red/violet/green resin. (core break).
KXTE2.d *	1.95 - 2.26	Continuation of fracture in c. Ends at about 2.10.
KXTE3.a	0.86 - 1.12	Contains intact fracture with small angle to core axis. Red/violet resin? Intersection with P7.
KXTE3.b	1.12 - 1.36	Continuation of fracture in a.
KXTE3.c	1.36 - 1.55	Continuation of fracture in b. Also crossing fracture with almost perpendicular orientation.

a)

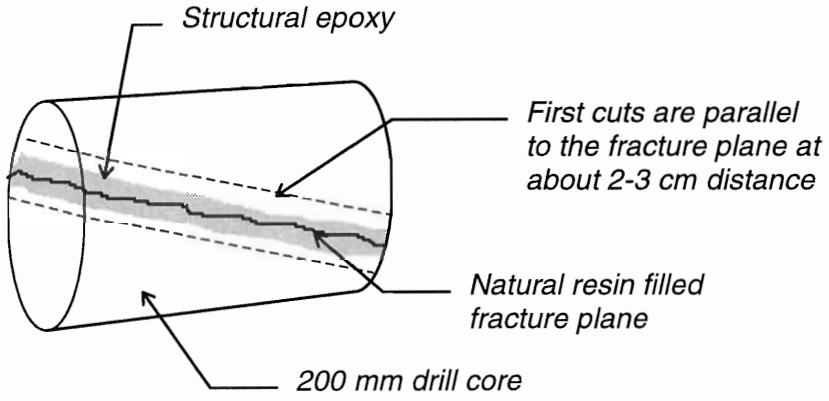

b)

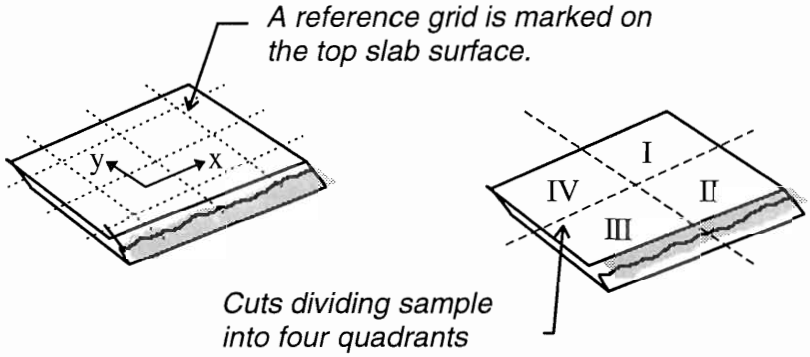

Figure 2-1 Illustrations of the sample preparation procedures (see text).

2.2 Data Profile Location

Plan sketches showing the location of each profile for Samples 1b and 3b are presented in Figures 2-2 and 2-3, respectively. Note that the profiles in Quadrants IV were measured using a photo-microscope technique (Section 2.4) and the profiles is the Quadrants I, II and III were measured using an image analysis technique (Section 2.5).

A total of 13 profiles were sectioned from Sample 1b, Quadrant IV, (7 in the X direction and 6 in the Y direction) and 16 from Sample 3b, Quadrant IV, (9 in the X direction and 7 in the Y direction).

In Quadrants I, II and III three profiles were sectioned in the X and Y directions, respectively. The surface coverage by the profiles in these quadrants is thus more widely spaced. Cost considerations limited the number of profiles that could be completed in this program.

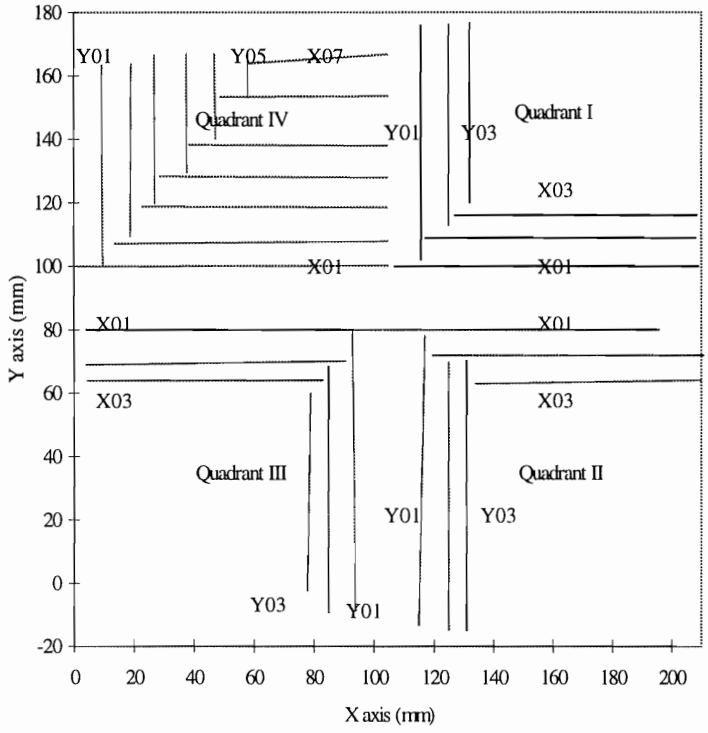

Figure 2-2 Location of measurement profiles on Sample 1b.

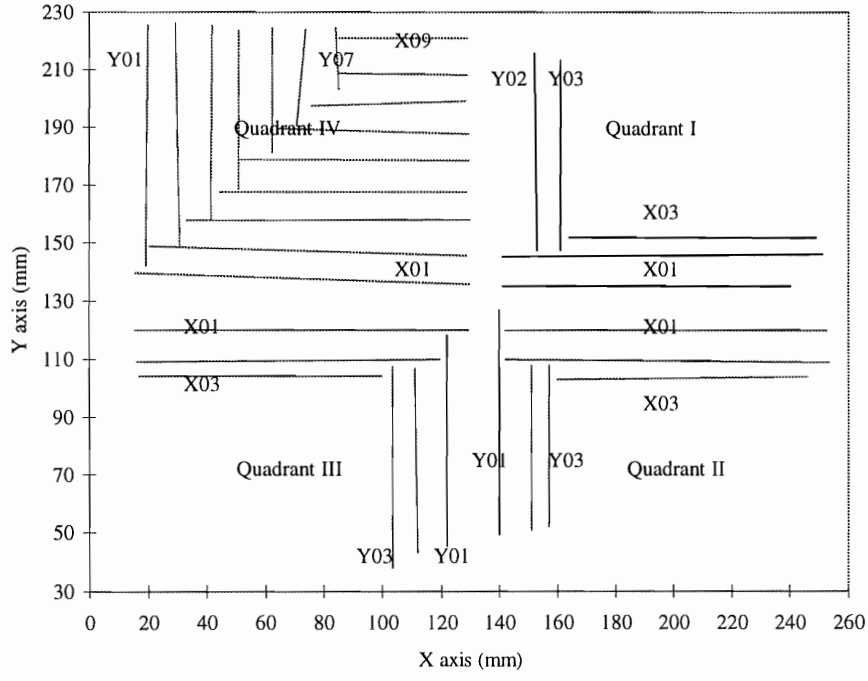

Figure 2-3 Location of measurement profiles on Sample 3b.

The reference grid was drawn on the same side of the rock slab as the side on which the drill core mapping reference line, used to orient the core, was drawn (i.e. on the top side of the core). The drill core axis lies in the x-z-plane of the fracture and the angle between x-axis and drill core axis (α) is 13.9 degrees, for Sample 1b, and 17.9 degrees, for Sample 3b (Birgersson et al., 1999). The x-coordinate increases with increasing depth of the drill hole. The fracture planes from which Samples 1b and 3b were taken are oriented 251/58 (strike/dip) and 12/88, respectively, based on the drill core mapping, see Figure 2-4.

a)

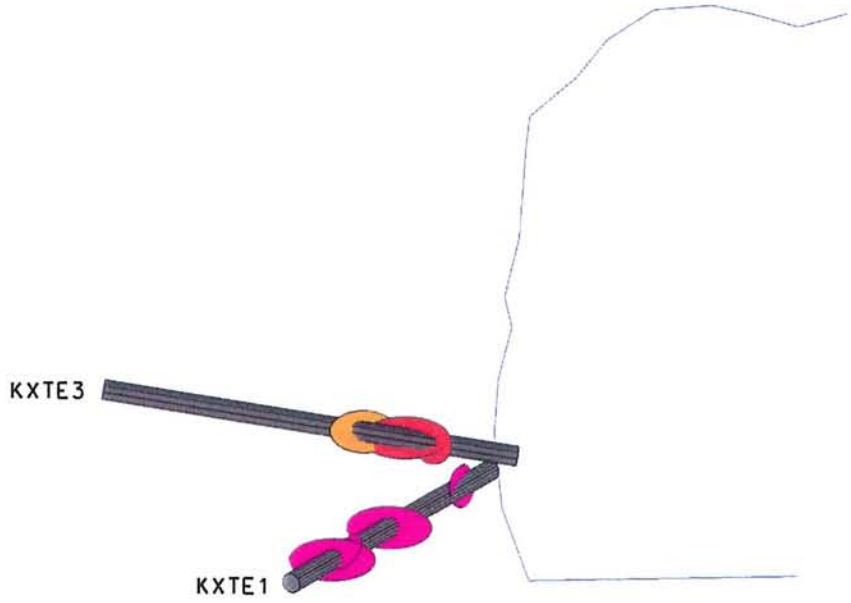

b)

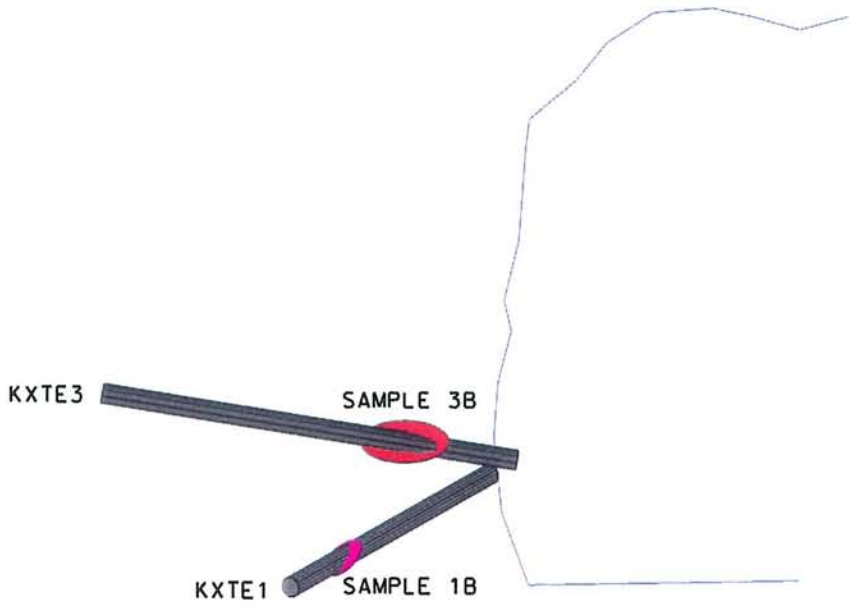

Figure 2-4 View of drift showing a) fracture planes intersecting boreholes KXTE1 and KXTE3 and b) resin filled planes sampled for pore structure analysis.

2.3 Definition of Mapped Entities

The thickness of the resin layer, at any given location, is calculated as the distance from the lower edge of the fracture or resin to the upper edge of the fracture or resin. This measurement is taken perpendicular to the average or mean direction of the profile length. If there is no detectable thickness of resin at the measurement point and the adjoining walls of the fracture appear to be touching, this point is recorded as a "contact point", and the aperture variable is assigned a value of zero. Also, the location of the upper and lower edges of the fracture walls at voids, where no resin has penetrated, are recorded. The accuracy of the measurements is about 0.02 mm for the magnification used in this case. (This accuracy is for the relative distances between points in the same picture).

Contact length is calculated as the distance, parallel to the length of the measurement profile, along which the measured upper and lower fracture surface data have the value zero. The accuracy of the contact lengths is thus 0.07 mm which is the distance between measurement points after the data are filtered.

To enable easy comparison, the data format of the measurements is the same for both the photo-microscope technique and the image analysis technique. The data-files contain information on the x- and y-coordinate of each data point, the height position of the upper and lower fracture surface, the aperture (or the resin thickness) and the length of each contact section.

Each data point has a code corresponding to the status of the point. Code 0 refers to "void", i.e. at this point there is no resin between the two surfaces. Code 1 stands for "resin", i.e. the fracture is filled with epoxy resin from the upper side to the lower. Code 2 stands for "contact" and refers to a point where there is no resin and also no void between the surfaces. This may be a point where the intact fracture surfaces touch each other or a point where some loose material (single fragment or filling material) fills up the space between the fracture walls.

At some parts of the profiles, a singular resin filled fracture trace splits up into two resin layers ("doubles") or the rock is crushed such that the pattern of resin is complex. At such points there will be more than one measurement "object" at the same profile length coordinate. These data are assigned code 3 (see also Section 3.1). A few data have Code 4 assigned which indicates that the accuracy of the measurement is low at this point. Also, at a few points the measurement data have been omitted because of low accuracy and the corresponding rows of data have been omitted from the data file.

2.4 Photo-Microscope Technique

Fracflow Consultants Inc. carried out resin thickness and/or aperture measurements using a photo-microscope, to provide enlarged images of the resin filled fractures, and a digitizer to provide the coordinates of the perimeter of the fracture pore space and the

location and lengths of the contact areas between the adjoining walls of the fracture surface.

Each profile was viewed under a microscope and a series of photographs were taken along each profile. Each photograph covered about 7 to 8 mm of the fracture length and a 2 to 3 mm section on either side of the fracture plane. The combination of the magnification of the microscope and the enlargement of the area by printing the photograph produced about a 1:18 enlargement of the resin filled fracture plane. The photographs were joined with about a 20% overlap to reduce edge distortion and taped to a paper backing.

The top and bottom of each fracture trace, contact points, and areas of resin filling and voids were then outlined by matching the photograph image with the microscope view. The upper and lower edges of the resin filled fracture plane were digitized by tracing the outlined fracture traces with the mouse of the digitizing tablet. Contact zones, voids (zones that were not filled with resin) and zones of crushed material, impregnated with resin, were digitized and classified separately. The resin thickness and fracture aperture were calculated from the digitized data as the distance from lower edge to upper edge, orthogonal to the profile axis. Measurements were made successively at points along each profile with a constant separation between the data points and the measurements were filtered during data processing to provide a measurement approximately every 0.07 mm.

2.5 Image Analysis Technique

Image analysis technique measurements were made by Itasca Geomekanik using the image analysis system IBAS at KTH. Automatic measurements were made using successive images grabbed from a video camera attached to a microscope. Between each image the sample was moved one image width under the microscope.

Measurement routines have been designed to detect the areas with resin (dark) in the image and to make a binary image, i.e. dividing the image into two categories only: fracture aperture and fracture side rock. In the binary images the position of lower and upper fracture surface is automatically measured at every 70 μm distance. With the magnification used in this case, each image corresponds to 3.5 mm profile length. Each image contains 1024x1024 pixels. The accuracy of the measurements increases with the quality of the image. Higher accuracy is achieved with a high magnification on the microscope and a large contrast between the epoxy and the fracture minerals. The digital images can be saved for documentation if desired.

3 Results

3.1 General Geological Description Of Samples

The mineralogy and texture of the two samples were examined using stereomicroscope and transmission microscopy on thin sections from selected parts of the fractures studied. The mineralogical identification reported in Section 3.1 was carried out by Eva-Lena Tullborg, Terralogica AB.

Both fractures, although different, are representative for the types of fractures usually observed at the Äspö HRL. Both of the studied fractures are hosted in Äspö diorite which is a quartz monzodiorite with 1-2 cm large K-feldspar phenocrysts.

3.1.1 Sample 1b

This fracture (251/58, strike/dip) belongs to a group of tension fractures that has fracture infillings consisting of idiomorphic calcite crystals. The occurrence of well preserved crystals in the analyzed sample indicates that the calcite has been able to crystallize in an open space and subsequent shear movements have not occurred (Figure 3-1a). The lack of obvious shearing is also supported by the observation of little to no displacement of e.g. K-feldspar phenocrysts transected by the fracture.

Apart from calcite, there is also pyrite in the fracture (Figure 3-1b). These mineralizations may be due to activities of sulfate reducing bacteria. Both past and present activity of such bacteria have been documented at Äspö (cf. Laaksoharju, 1995). Another possibility is a hydrothermal origin of the pyrite and possibly the calcite as well. Without stable isotope analyses of sulfur, carbon and oxygen isotopes from the calcite and pyrites it is not possible to determine their origin in this case.

In addition to calcite and pyrite, which dominates the coating, quartz and K-feldspar crystals have grown at some places along the fracture.

The wall rock consists of Äspö diorite which is partly sericitised and show weak red staining of the feldspars due to precipitation of minute grains of K-feldspar.

The main part of the fracture consists of one single fracture layer with a fairly constant aperture (Figure 3-1c). However, at some points the fracture branches into two "layers", or the surface rock is fragmented into even more complex patterns (Figure 3-1d). This seems to occur at the "bridging" points of very close subparallel fracture traces.

The surfaces of Sample 1b are fairly rough and slightly offset, which can be noted mainly in the profiles in the x-direction (Figure 3-1c and e). The estimated magnitude of the displacement in the x-direction is 250 -350 μm and about 50 μm in the y-direction.

The resin impregnation of the fracture in Sample 1b is complete and there is very little contact between the fracture surfaces (see further Sections 3.2-3.5). The colour of the resin is slightly pink/violet probably due to the Rhodamine dye injected prior to the resin, see (Birgersson et al., 1999). The resin is transparent and therefore appears dark in the sample sections. At some point the resin can be difficult to distinguish from the darker minerals (Figure 3-1f).

a)

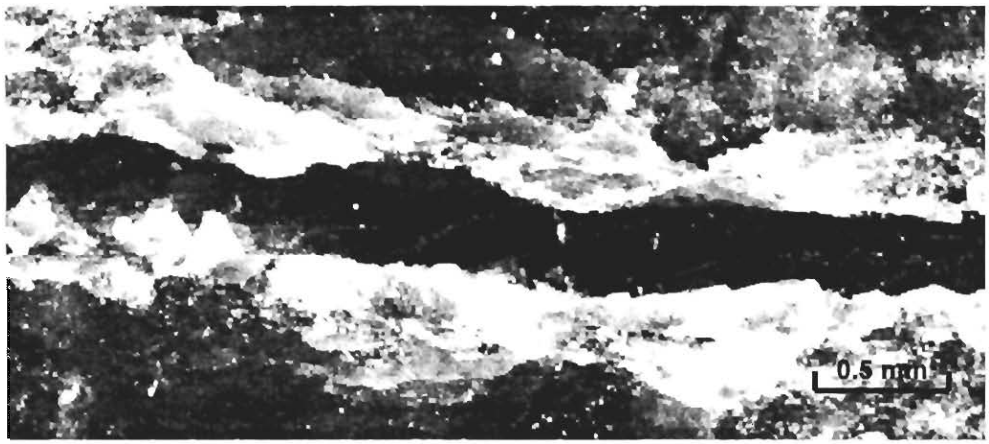

b)

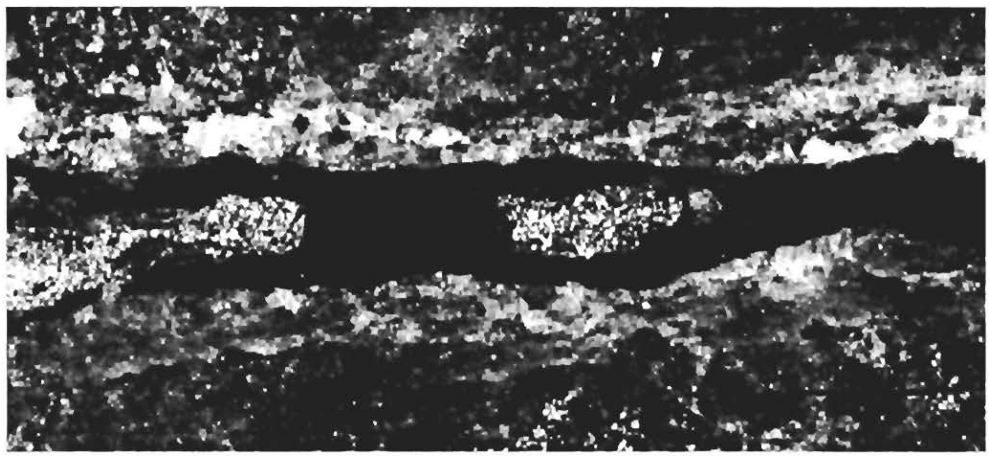

Figure 3-1 Image examples from Sample 1b. a) Calcite mineralization inside fracture. b) Pyrite mineralization. c) Typical section from Sample 1b. Fairly constant aperture. Fairly rough fracture surfaces. d) Complex pattern of the fracture aperture due to breakage of the fracture side rock. e) Upper surface indicates about 270 μm displacement to the left in the x-direction.(See black arrows). f) Dark mineral (white arrows) has low contrast to resin and it will at some points be difficult to make an accurate measurement. Therefore automatically identified distances (thicknesses) were manually checked and corrected on all images as needed.

c)

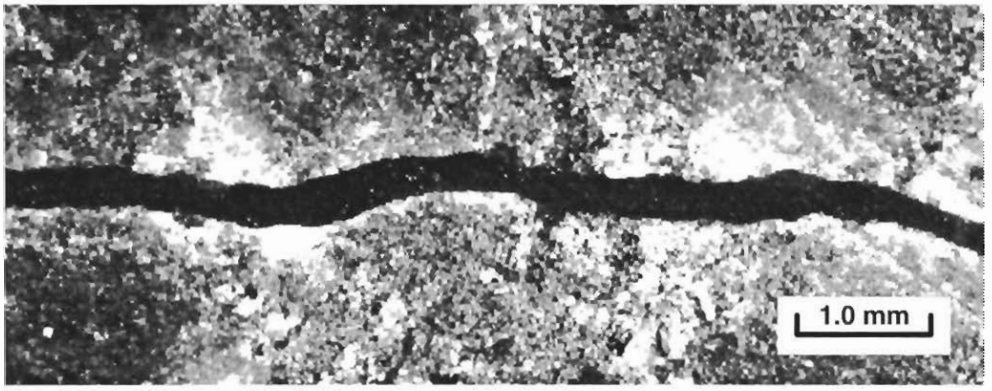

d)

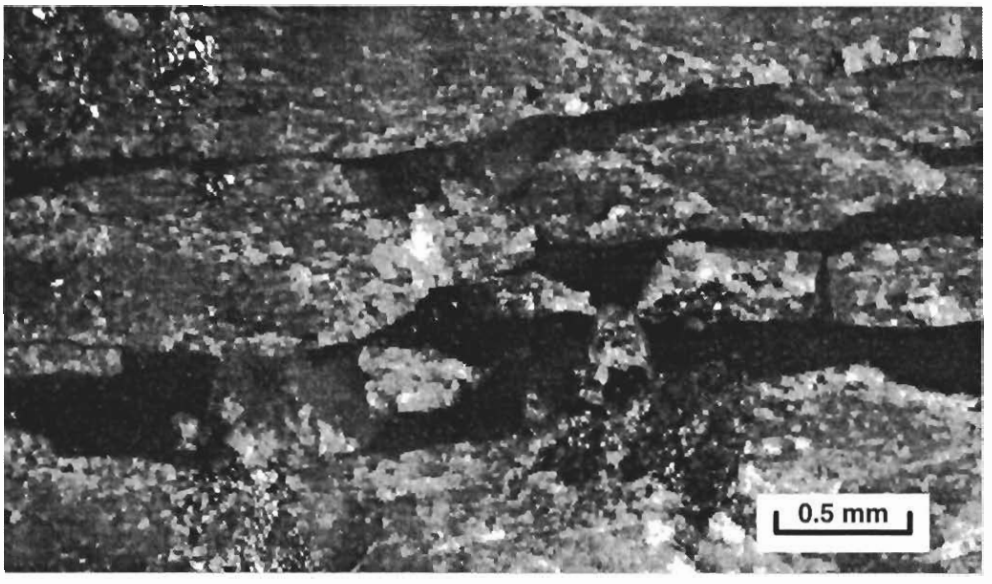

e)

f)

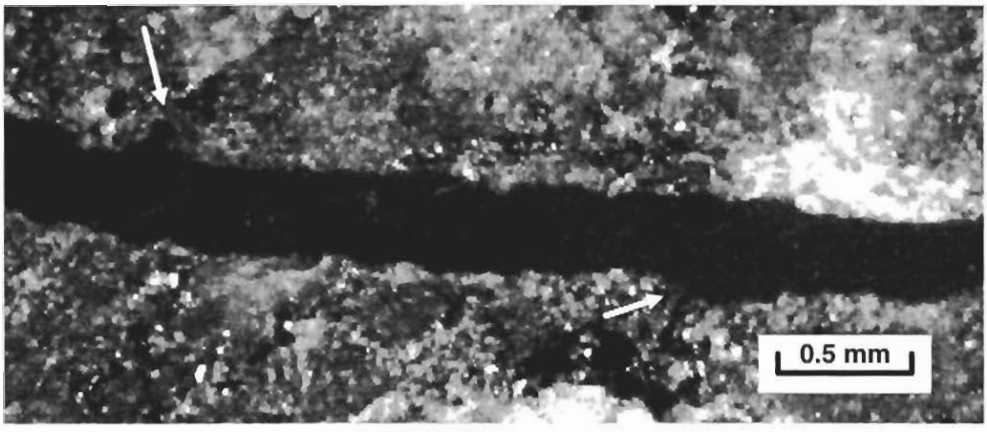

Figure 3-1 Sample 1b (continued) See figure caption on page 11.

3.1.2 Sample 3b

Sample 3b fracture (12/88, strike/dip)is from another group of fractures that has been observed at Äspö, which are generally characterized by hydrothermal alteration of the adjacent wall rock. This is demonstrated in this fracture sample by the breakdown of biotite to form chlorite, saussuritisation of the plagioclase and breakdown of magnetite to form hematite. The latter is responsible for the red staining shown as a 5 mm thick rim along the fracture. The fracture studied has experienced shear movements which is seen as relative displacement along the fracture.

The fracture filling material consists mostly of rock fragments of different sizes. The coarser material is mainly feldspar and quartz. The finer material has, in addition to K-feldspar and quartz, also a large percentage of chlorite/corrensite. The shape and appearance of the crushed material indicate that it did not form recently. Some grains even show rims of alteration products. Some single crystals of calcite and pyrite have grown inside the fracture. The ages of these crystals are not known but they may have formed relatively recent, i.e. much younger than the formation of the fracture itself or the altered rock fragments.

Generally the fracture surfaces of Sample 3b are smooth and the aperture is fairly constant, except in the areas with infilling material (Figure 3-2a). The extent of filled areas (here referred to as "contact areas") is much larger in Sample 3b as compared to Sample 1b (Figure 3-2b and d). Also, a portion of Sample 3b consists of void spaces or areas not filled with resin (Figure 3-2c). These voids or unfilled pore spaces are interpreted to represent either dead-end pore space or pore space that is filled with trapped fluid, which does not contribute to flow through the fracture, or the result of a failure to fully impregnate the fracture with resin. The voids are often located between contact areas (See further details on voids in Section 3.1). Some air bubbles, or pockets of trapped air, are also observed in the resin sections (Figure3-2d).
Since the infilling material, or gouge, is mainly loose unconsolidated material it is not clear if it has been transported into the fracture or displaced during the hydraulic testing

and resin impregnation activities. The impression from the thin section studies is that the infilling material has not moved significantly. However, single loose crystals might have moved very short distances. The fact that some parts of Sample 3b is filled completely with fine-grained material also indicates that there may not have been any significant fracture opening due to the injection pressures, which generally were in the range 1-2 MPa. *In situ* formation of the observed loose material in the fracture is generally supported by the thin section observations.

a)

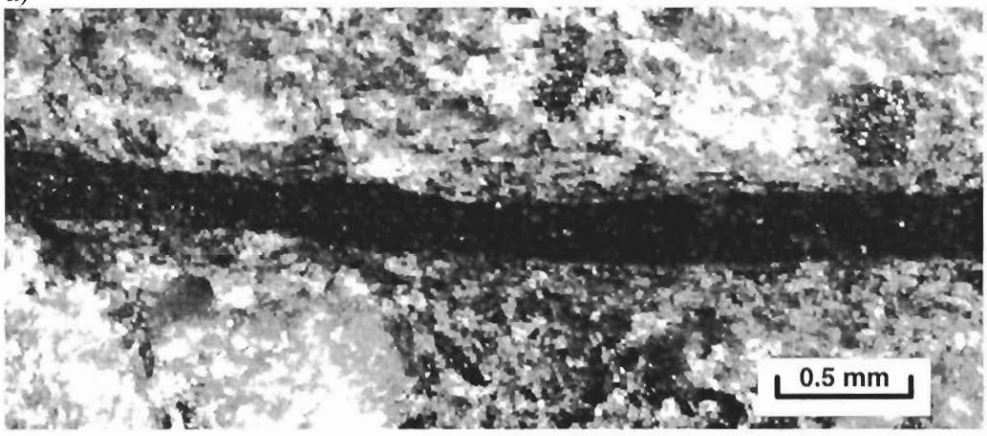

b)

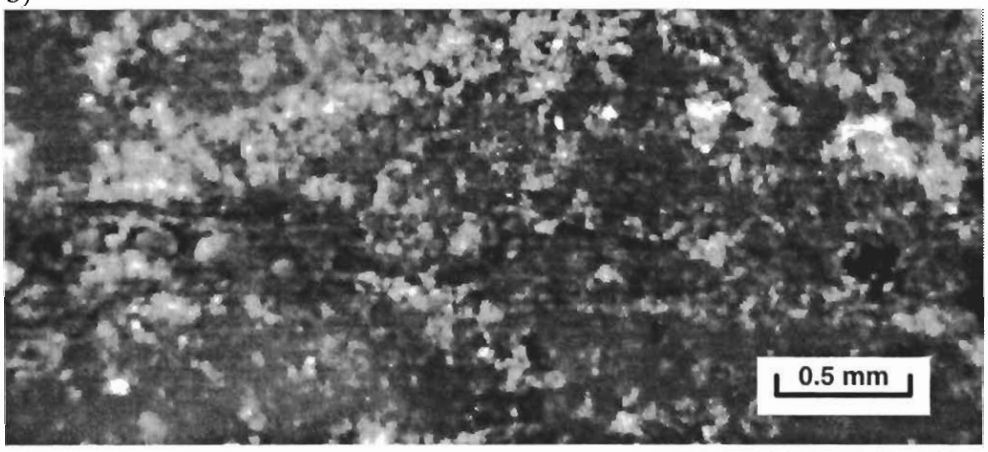

Figure 3-2 Image examples from Sample 3b. a) Typical section in area without contacts. Fairly constant aperture between contacts. Smooth surfaces. b) Typical section in large contact area. The border of the intact rock surface is difficult to distinguish. The material making up the contacts has grains of different sizes and also pores, some of which are resin filled. c) In the section with voids it may be difficult to determine the correct surface location. Also, the fracture section may become damaged during the sample preparation and small loose rock fragments may disappear. d) Epoxy-filled aperture on left side and contact area on right side. The resin contains air bubbles to a limited extent. Within the contact sections resin has sometimes penetrated in thin layers or pores. This type of small isolated resin occurrence has normally been interpreted as contact. This figure exemplifies the typical abrupt change in aperture found in Sample 3b.

c)

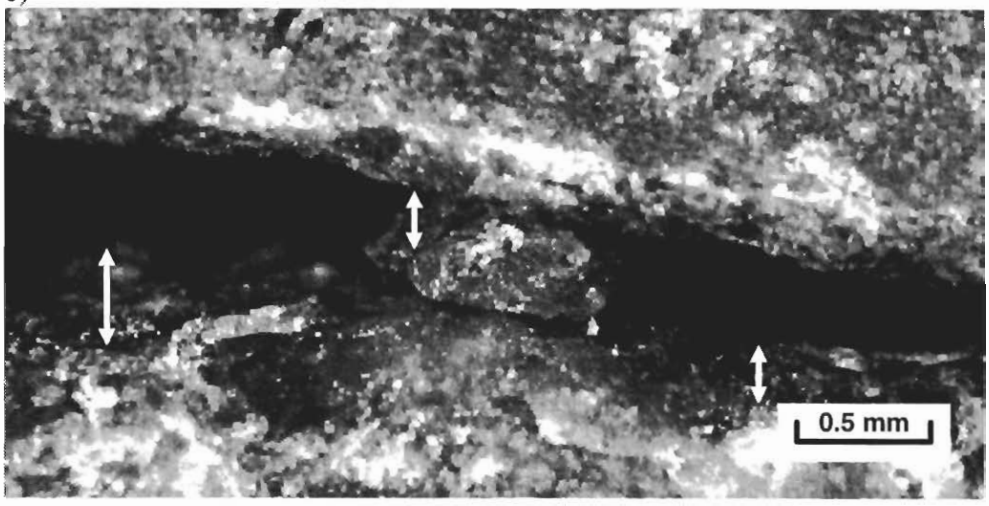

d)

Figure 3-2 Sample 3b (continued) See figure text on previous page.

3.1.3 Sample 2c

When Sample 2c was drilled the fracture was broken. In order to rescue this sample it was glued together with a transparent epoxy without dye. After the sample preparation it was observed that it was not possible to distinguish between the epoxy used in the *in-situ* injection and the epoxy used to glue the fracture back together. It was therefore decided to make no further measurements on this sample, since the measurement uncertainties would be too large.

The geological characters of Sample 2c seemed to be similar to what was seen in Sample 1b.

3.2 Summary Statistics

Tables 3-1 and 3-2 present statistics for profiles from Samples 1b and Sample 3b, respectively. Quadrants I-III were measured using the image analysis technique and Quadrant IV using the photo-microscope technique. Statistical parameters include contact length, percentage of contact length, mean aperture and a coefficient of variation for each profile (coefficient of variation is defined as standard deviation divided by the mean). Statistics have been calculated for the complete profile (including contact, void and resin areas) and for sections with resin occurrence alone. The main results for each sample are discussed in the following sections.

3.2.1 Sample 1b

The mean apertures for all data from profiles in Sample 1b range from 178 μm to 336 μm while the coefficients of variation range from 20% to 64%. The variability for the mean aperture for the areas with a single resin layer is almost the same, 206 - 337 μm with coefficient of variation varying from 20% to 52%. The difference is small since most of the fracture pore space is penetrated with epoxy resin and there is mainly one single resin layer. In Figure 3-3 the coefficient of variation for each profile (resin areas) is plotted against the mean aperture. In this diagram it can be noted that the spread of points is fairly similar, irrespective of the sample quadrant, i.e. there is no major difference in the aperture variation in different parts of the sampled fracture surface. The location of profiles are given in Figure 2-2. It should, however, be remembered that the total area studied is very small compared to the estimated total fracture area (<1%).

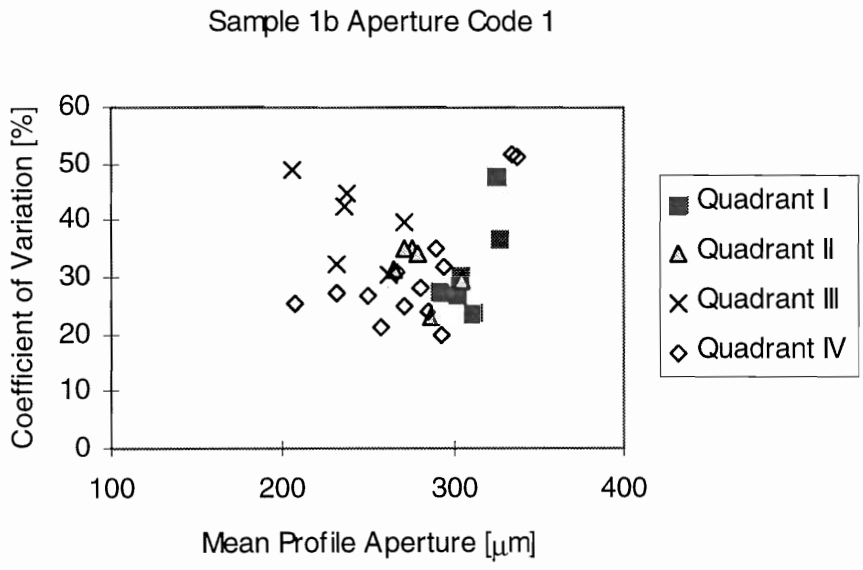

Figure 3-3 Diagram with coefficient of variation (St. Dev. / mean) versus the mean aperture for the measurement profiles of Sample 1b. Only apertures in Resin impregnated areas are included (Code 1). Ther is no obvious grouping or clustering of the averages from quadrant to quadrant.

3.2.2 Analysis of sensitivity in Sample 1b univariate statistics

For one part of a profile, a comparison was made between results from repeated measurements with different measurement conditions, using the image analysis technique. The profile length was about 41 mm starting from the lowest x-coordinate of 1bII X01. The magnification normally used (ST2) and a 70 μm distance between data points gave a mean aperture of 268 μm and a standard deviation of 57 μm. There were 584 data points in this data set.

Using a magnification of the images that was half as large (ST1), but keeping the same measurement separation distance (70 μm), resulted in a mean aperture of 263 μm with a standard deviation of 56.4 μm. The locations of the actual measurement points should be almost the same as in the previous case, but since the magnification differs, and the accuracy of the measurement location is limited by the pixel size, the locations are not identical. Also the starting point might be slightly different. In addition, the lighting conditions change when using a different magnification, and it is harder to get a good and even light with high magnification. On the other hand, the objects to be measured are of course larger using high magnification, improving the accuracy.

The stability of measurement results are further demonstrated by the results from measurement with the lower magnification (again ST1) but with 200 μm separation between measurement points. The mean aperture then becomes 267.0 μm with a standard deviation of 56.6 μm. The total number of points in this data set was 210, about three times less than the two previous data sets where the separation distance was 70 μm.

This comparison indicates that the aperture distribution parameters are insensitive to the changes in measurement conditions. The choice of magnification and measurement point or data separation therefore can be based on the particular application of the data and on the time and cost limitations. High accuracy might be more important in cases with small apertures. Short data separation might be needed when the spatial correlation is small and when details of the surface topography are to be studied. The number of images, i.e. the magnification, is the main factor controlling the time needed for measurement on a sample profile.

Table 3-1 Statistics on profiles of Sample 1b. Quadrants I-III were measured using the image analysis technique and Quadrant IV using the photo-microscope technique. For definition of measured entities see section 2.3.

Profile				All data Aperture			Resin Aperture			Contact		Incl.	Void	Resin
name		length (mm)	no of data	mean (μm)	St.D. (μm)	CV %	mean (μm)	St.D. (μm)	CV %	length %	no of cont.	length %	data %	data %
1bI	X01	102	1615	278	105	38	302	82	27	0.2	2	10	0	82
	X02	91	1321	293	103	35	303	92	30	0.7	4	2	0	96
	X03	81	1231	266	101	38	291	81	28	0.9	5	7	0	86
	Y01	74	1294	277	144	52	326	120	37	0.9	6	21	0	64
	Y02	63	908	310	75	24	311	74	24	0.0	0	0	0	100
	Y03	57	899	289	162	56	325	157	48	0.4	2	11	0	80
1bII	X01	93	1351	281	76	27	286	66	23	0.0	0	3	0	94
	X02	91	1620	246	128	52	305	89	29	0.3	2	20	0	66
	X03	76	1091	252	118	47	277	97	35	6.1	5	2	0	88
	Y01	92	1362	258	105	41	272	95	35	0.5	5	4	0	92
	Y02	85	1218	255	95	37	266	84	31	2.7	9	2	0	94
	Y03	85	1222	268	104	39	278	95	34	0.7	7	3	0	94
1bIII	X01	98	1453	229	111	48	238	106	45	1.1	11	3	0	94
	X02	86	1301	220	83	38	232	75	32	0.5	4	5	0	89
	X03	78	1162	223	109	49	236	101	43	2.2	13	5	0	89
	Y01	89	1498	238	119	50	262	79	30	0.5	4	7	0	72
	Y02	78	1140	178	114	64	206	101	49	9.5	20	3	0	73
	Y03	62	1042	233	125	53	272	108	40	0.7	4	15	0	73
1bIV	X01	104	1470	334	173	52	334	173	52	0.0	0		0	100
	X02	91	1336	285	68	24	285	68	24	0.0	0		0	100
	X03	82	1164	336	172	51	337	172	51	0.1	1		0	100
	X04	76	1099	294	94	32	294	94	32	0.0	0		0	100
	X05	66	965	294	59	20	294	59	20	0.0	0		0	100
	X06	56	818	289	102	35	289	102	35	0.0	0		0	100
	X07	47	681	266	85	32	267	83	31	0.3	1		0	99
	Y01	63	908	280	79	28	280	79	28	0.0	0		0	100
	Y02	54	784	257	55	21	257	55	21	0.0	0		0	100
	Y03	46	665	250	67	27	250	67	27	0.0	0		0	100
	Y04	38	542	272	67	25	272	67	25	0.0	0		0	100
	Y05	27	388	231	63	27	231	63	27	0.0	0		0	100
	Y06	13	196	207	53	25	207	53	25	0.0	0		0	100

Table 3-2 Statistics on profiles of Sample 3b. Quadrants I-III were measured using the image analysis technique and Quadrant IV using the photo-microscope technique. For definition of measured entities see section 2.3.

Profile				All data Aperture			Resin Aperture			Contact		Incl.	Void	Resin
name		length (mm)	no. of data	mean (µm)	St.D. (µm)	CV %	mean (µm)	St.D. (µm)	CV %	length %	no. of cont.	length %	data %	data %
3bI	X01	99	1422	265	134	51	319	69	22	16	9		1	82
	X02	110	1586	237	174	73	324	88	27	29	16	0.1	20	51
	X03	85	1234	203	218	108	306	102	33	41	7	0.5	9	49
	(Y01)												0	0
	Y02	68	1009	198	163	82	283	75	27	29	20	0.1	36	35
	Y03	66	938	154	148	96	272	73	27	43	12	0.4	34	24
3bII	X01	110	1583	269	142	53	322	85	26	16	13	0.4	0	83
	X02	111	1629	257	168	65	339	106	31	21	12	1.7	2	74
	X03	86	1273	293	145	49	334	100	30	9	5	3.6	4	80
	Y01	78	1151	226	188	83	333	111	33	31	11	0.0	28	42
	Y02	57	827	192	183	95	285	127	45	36	5	0.0	13	52
	Y03	56	792	294	222	75	328	92	28	21	12	0.0	21	58
3bIII	X01	114	1632	172	137	80	255	80	31	33	14	0.0	4	63
	X02	103	1491	111	150	135	261	130	50	56	26	0.5	8	36
	X03	83	1205	110	142	129	227	97	43	55	16	0.0	8	36
	Y01	73	1150	249	175	70	308	83	27	17	15	0.0	42	43
	Y02	64	1024	257	159	62	294	99	34	10	13	0.7	38	52
	Y03	69	1021	211	200	95	381	123	32	40	13	2.7	15	41
3bIV	X01	114	1633	247	147	59	278	176	38	15	6		9	76
	X02	108	1545	249	150	60	275	73	27	16	9		14	69
	X03	96	1404	302	116	38	290	89	31	4	2		25	71
	X04	84	1256	490	186	38	500	208	42	0	0		44	56
	X05	78	1108	339	136	40	355	116	33	0	1		73	26
	X06	65	949	255	145	57	246	91	37	10	4		29	60
	X07	53	755	175	111	63	206	66	32	19	3		7	74
	X08	44	613	217	135	62	267	95	36	17	4		0	81
	X09	43	594	259	119	46	286	88	31	9	1		0	90
	Y01	83	1216	226	162	71	196	107	55	14	7		32	54
	Y02	77	1119	229	147	64	236	75	32	17	5		23	60
	Y03	67	972	169	133	79	207	99	48	26	5		28	46
	Y04	55	795	289	133	46	299	105	35	7	1		39	54
	Y05	43	617	269	161	60	258	83	32	17	4		43	39
	Y06	33	484	201	174	87	296	118	40	33	3		7	60
	Y07	22	315	157	92	58	186	68	36	14	2		0	84

3.2.3 Sample 3b

From Table 3-2, it can be seen that the mean aperture calculated for all data in profiles from Sample 3b ranges from 110 μm to 490 μm with coefficients of variation's ranging from 38% to 135%. The corresponding figures, if only the areas with resin are considered, are 186 μm to 500 μm for the mean, and 22% to 55% for the coefficient of variation.

In the same way as for Sample 1b, the aperture variation of Sample 3b is illustrated in Figure 3.4 with a plot of coefficient of variation versus mean aperture for each profile. Also for this sample the data plot in a cluster, and there is no clear difference in the spread between different quadrants of the fracture sample area. Since this sample has a large amount of contacts and voids, it should be noted that the apertures in the diagram refer to the resin impregnated areas only (See sections 3.4 and 3.5 for extended analysis of void and contact areas).

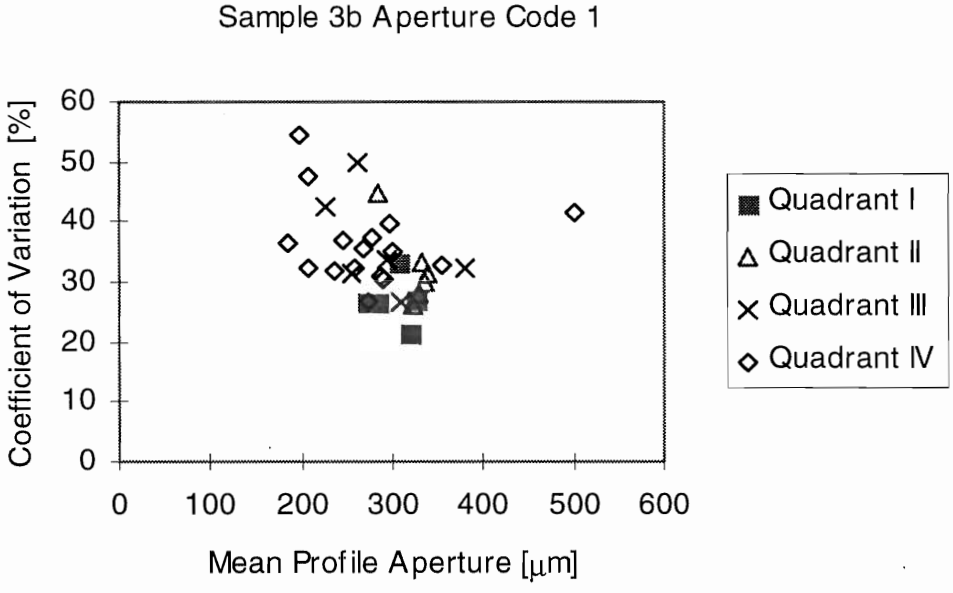

Figure 3-4 Diagram showing coefficient of variation (St. Dev. / mean) versus the mean aperture for the measurement profiles of Sample 3b. Only apertures in resin impregnated areas are included (Code 1).

3.2.4 Sample and sample quadrant summary statistics

Table 3-3 summarizes the statistics for each quadrant and the total sample, for both samples. For each quadrant and for the total, the data from the profiles are lumped together and the statistics calculated on all data. Quadrants I-III were measured using the "image analysis technique" and the Quadrant IV using the "photo-microscope technique". From Table 3-3 it can be noted that the mean aperture is fairly stable between quadrants in both samples. No major differences can be seen between results obtained using the different methods.

The mean aperture in the resin impregnated areas is in the same order for both samples, 281 μm and 295 μm, respectively. Also the standard deviation of the aperture is in the same order for both fractures, 37% and 39%. The difference in character between the two samples is revealed from the larger percentage of contact areas for Sample 3b, and also a larger percentage void area for this sample. From Tables 3-1 and 3-2 it can also be noted that the number or amount of inclusions (rock fragments, branching) is significantly less in Sample 3b.

Table3-3 Summary statistics of data from complete samples and sample quadrants.

Fracture Sample	Mean Aperture Resin [μm]	Standard Deviation Resin [%]	Contact Area [%]	Void area [%]	Mean Aperture All data [μm]
1bI	308	33	0.5	0	284
1bII	280	32	1.6	0	260
1bIII	240	41	2.3	0	221
1bIV	290	39	0.02	0	289
1bTotal	**281**	**37**	**1.0**	**0**	**266**
3bI	310	27	31	18	218
3bII	327	31	21	9	258
3bIII	282	39	37	17	179
3bIV	278	46	13	27	268
3bTotal	**295**	**39**	**22**	**20**	**239**

3.3 Aperture Distribution

Frequency histograms of apertures are shown in Figures 3-5, 3-6, 3-7 and 3-8. For each histogram, the mean, median, standard deviation, coefficient of variance, maximum and minimum, and the upper and lower quartile of the resin thickness, in micrometers, are

calculated and plotted along with the histograms. For comparison, histograms of the resin thickness or apertures, including the contact areas plus voids, have been plotted in Figures 3-5 and 3-6 for each quadrant for both Sample 1b and Sample 3b. The histograms on the left in these two figures contain the data for the parallel resin layers or "doubles" and the histograms on the right contain only the resin thickness and voids. The differences between the contact areas for Sample 1b and Sample 3b are obvious when the these histograms are compared.

The last two histograms in each of Figures 3-5 and 3-6, for Quadrant IV, are repeated in Figure 3-7 to provide a direct comparison between the two samples. In addition, the last two histograms in Figure 3-7 show the distribution of the logarithm of the resin thickness and voids or apertures without contact areas or "doubles" for Quadrant IV. Similarly, Figure 3-8 shows the histograms for the different combinations of resin thickness, voids, contact areas and "doubles" for all four quadrants. The generally symmetrical nature of the distribution of the logarithm of apertures, without the contact areas, for Sample 1b suggests that the apertures are log-normally distributed. However, the distribution of the logarithm of apertures for Sample 3b is skewed and does not appear to follow a log-normal model as closely as Sample 1b (See geological description of fractures in Section 3.1).

3.4 Contact Areas

The results of the contact measurements, as given in Table 3-1, Table 3-2 and Figures 3-5 to 3-8, show that the amount of contact area varies significantly between the two samples. Sample 1b has only a few contact points representing a contact length of approximately 1 % of the total of all profile lengths. The percentage contact is larger for Quadrants 1bI-III than for 1bIV. This might be explained by the different measurement techniques used, because the image analysis technique is expected to detect very small contacts (stuck fragments) to a higher degree than the photo-microscope technique. The typical contact points in Sample 1b are only 100 to 200 μm long.

In contrast, Sample 3b has a large percentage of contact. The contact length calculated for all data from Sample 3b is 22 % of the total of all profile lengths. The variation between profiles is large; from 0% up to 56% for different profiles from the same fracture sample. Figure 3-9 shows a diagram which illustrates the variation in the percentage of contact for each quadrant of Sample 3b. It can be noted that Quadrant IV has a smaller percent of contact than the other three. This can be explained by differences in the measurement method, or differences in the interpretation of the fracture during measurement. However, it may also be explained by a true variation in contact occurrence over the fracture area, which is more likely the case since the range of contact values partly overlap for all four quadrants.

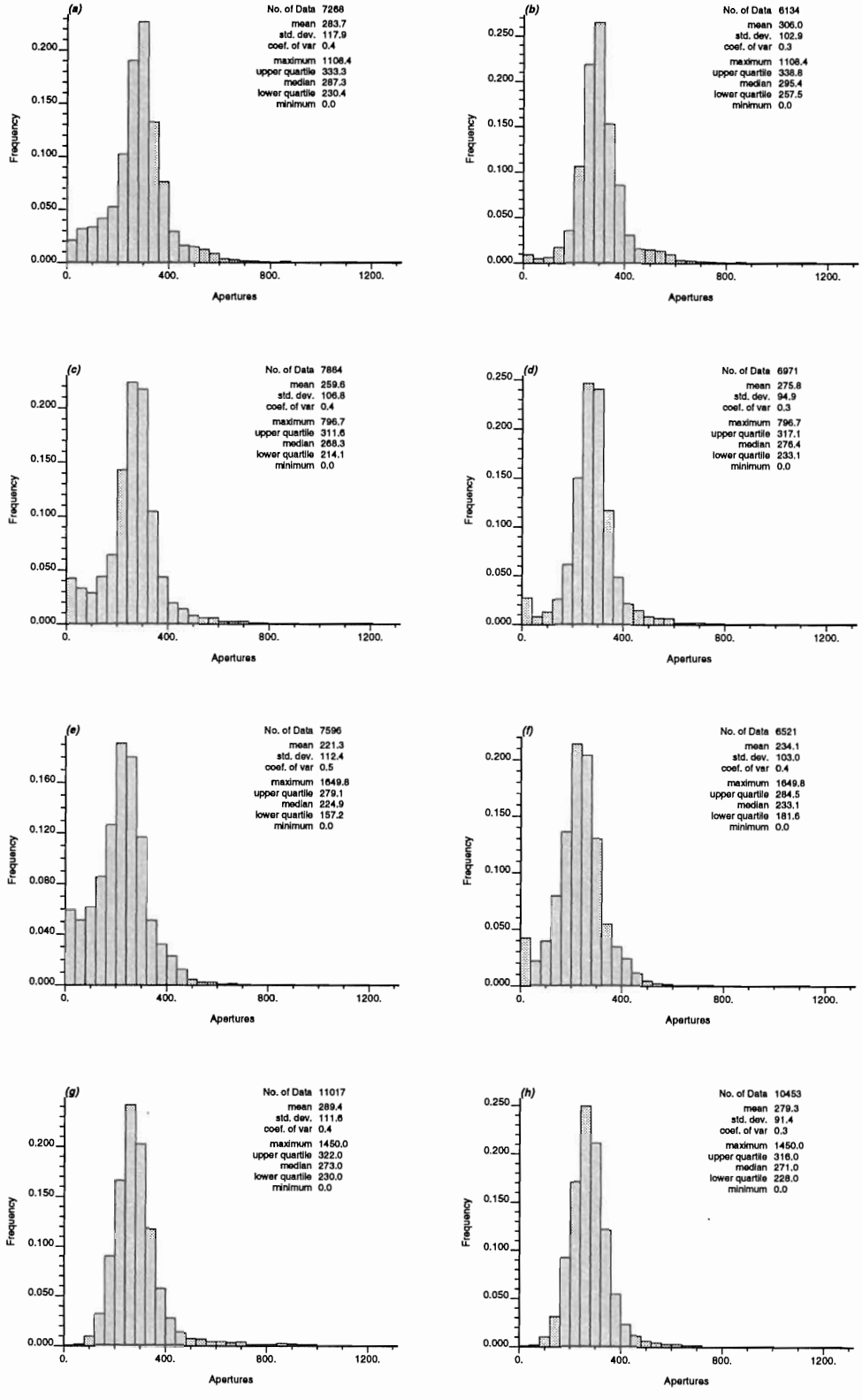

Figure 3-5 Histograms showing aperture (μm) distribution of Sample 1b. (a) and (b) represent Quadrant I with and without "doubles"; (c) and (d) Quadrant II with and without "doubles; (e) and (f) Quadrant III with and without "doubles"; and (g) and (h) Quadrant IV with and without "doubles". Contact areas are included.

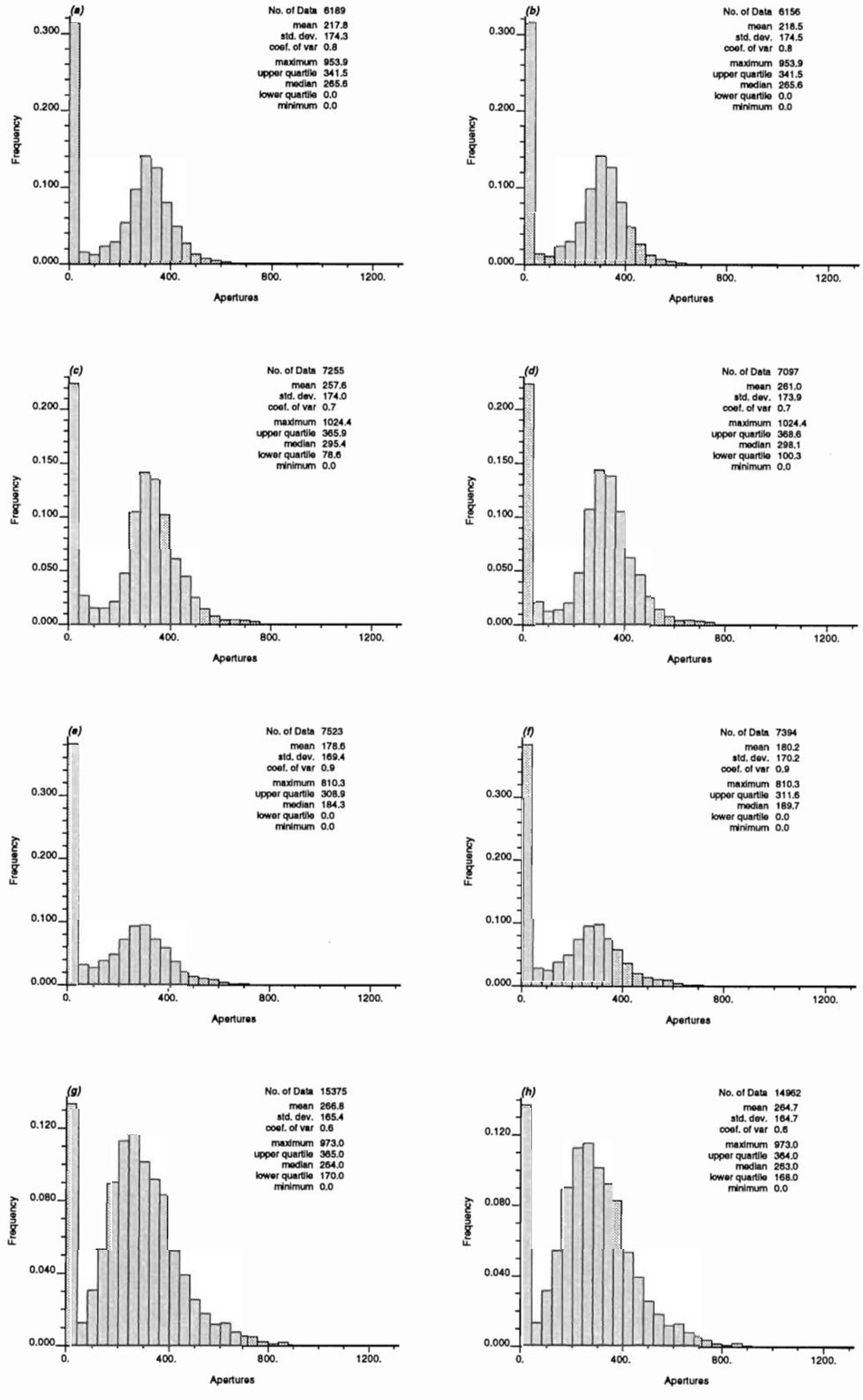

Figure 3-6 Histograms showing aperture (μm) distribution of Sample 3b. (a) and (b) represent Quadrant I with and without "doubles"; (c) and (d) Quadrant II with and without "doubles; (e) and (f) Quadrant III with and without "doubles"; and (g) and (h) Quadrant IV with and without "doubles". Contact areas are included.

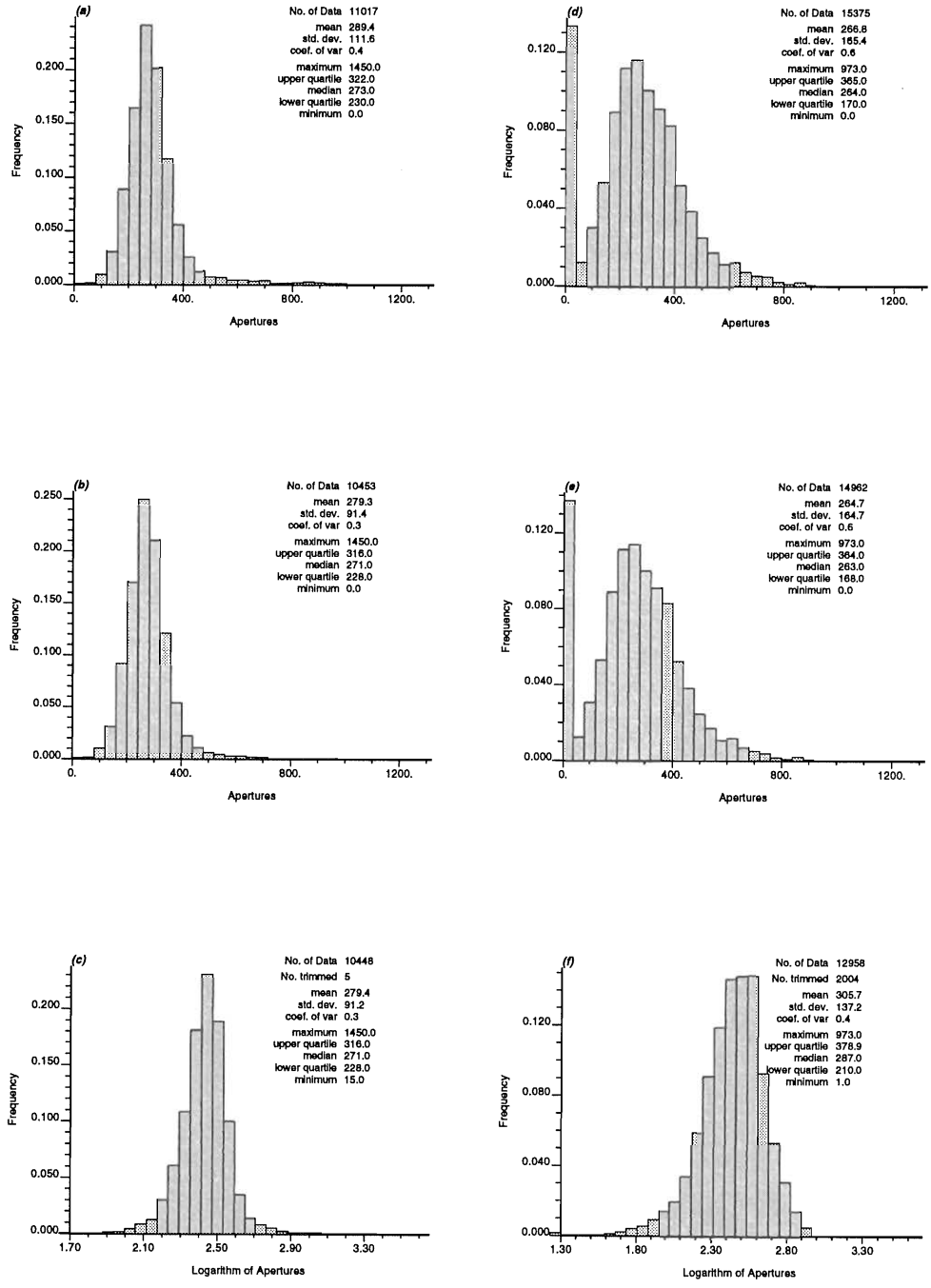

Figure 3-7 Histograms showing aperture (μm) distribution of Sample 1b Quadrant IV. (a) with both "doubles" and contact areas; (b) without "doubles", but with contact areas; and (c) logarithm of apertures with neither "doubles" or contact areas. Sample 3b Quadrant IV (d) with both "doubles" and contact areas; (e) without "doubles", but with contact areas; (f) logarithm of apertures with neither "doubles" or contact areas.

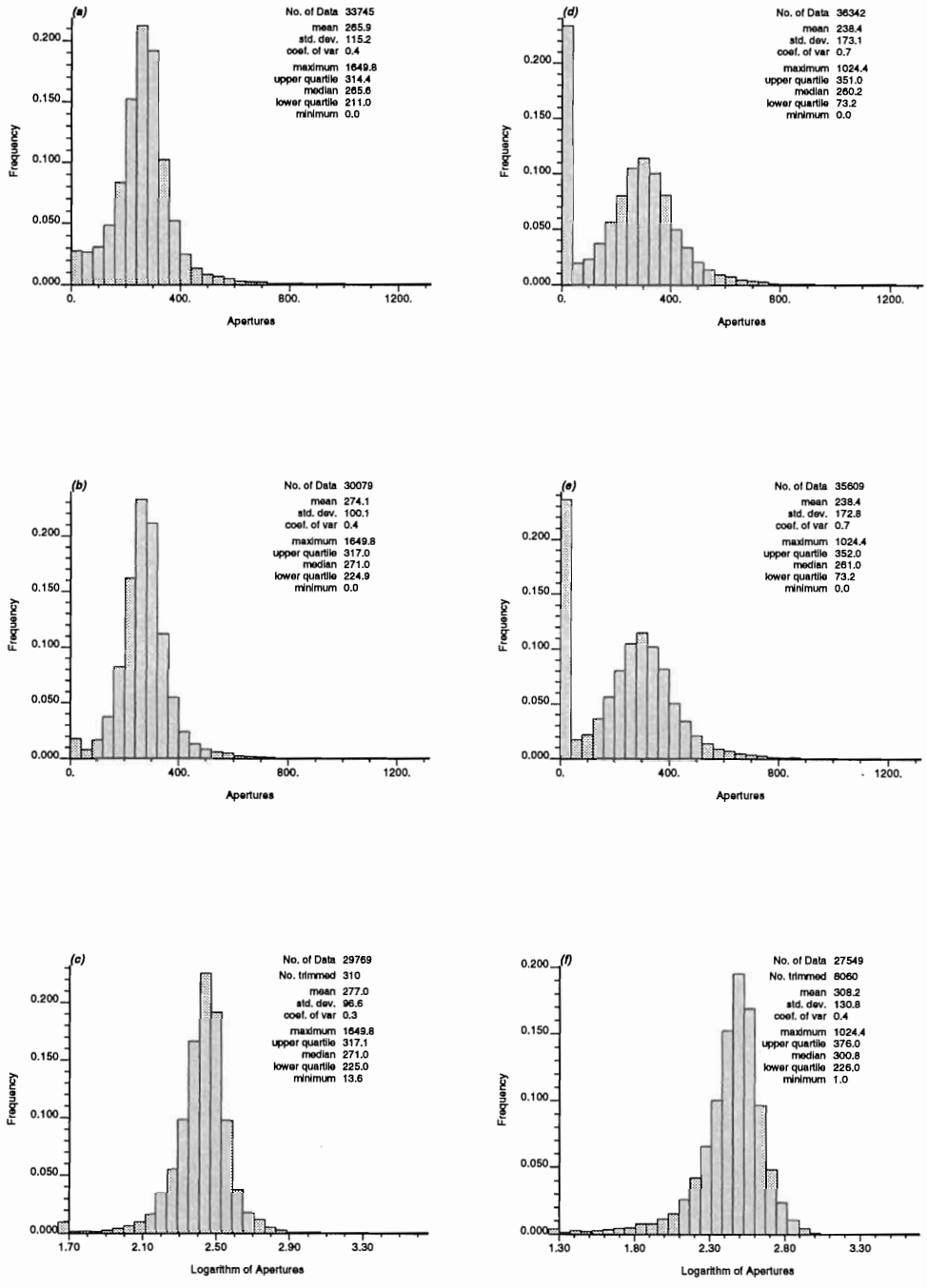

Figure 3-8 Histograms showing aperture (μm) distribution of Sample 1b. (a) with both "doubles and contact areas; (b) without "doubles", but with contact areas; and (c) logarithm of apertures neither "doubles" or contact areas. Sample 3b (d) with both "doubles" and contact areas; (e) without "doubles", but with contact areas; (f) logarithm of apertures with neither "doubles" or contact areas.

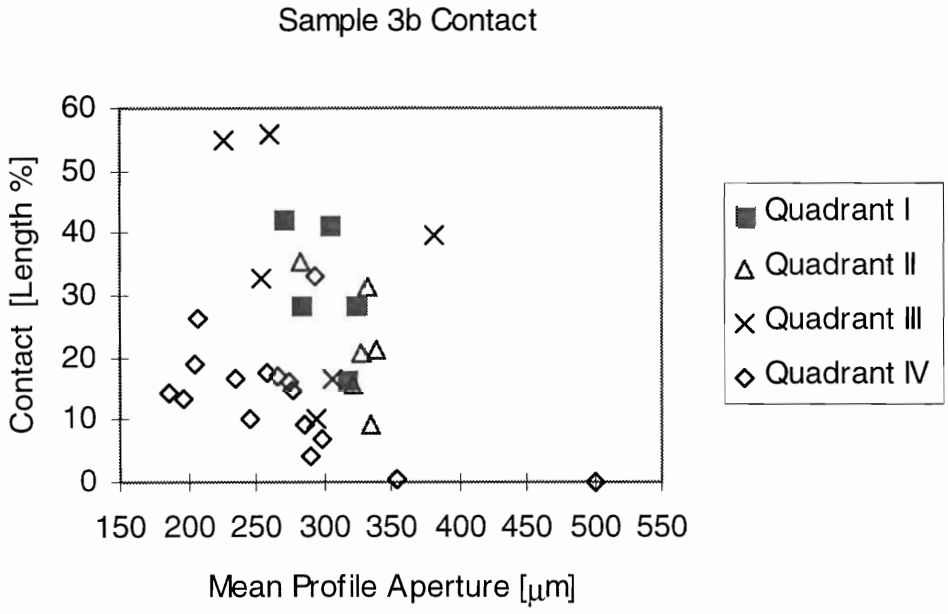

Figure 3-9 The amount of contact in each profile of Sample 3b, expressed as a percent of profile length, versus the mean aperture for each profile.

3.5 Void Areas

In Sample 1b the aperture geometry is often complex due to rock fragment inclusions and branching. Still this has not hindered the resin from fully penetrating into this sample. On the other hand, Sample 3b is not fully filled with epoxy resin although it has apertures in the same order of magnitude as Sample 1b, and fairly smooth fracture surfaces. The results thus indicate that void areas occur mainly due to the existence of contact areas that block the pathways and prevent the resin from penetrating fully into the fracture.

These results generally show that the mean aperture in void areas is larger than the mean aperture of the resin layer in the same profile (Figure 3-10). This may have two explanations, 1) the fracture surface edges break during sectioning and grinding such that the aperture becomes larger than in the undisturbed situation because there is no resin to support the edges of the fracture, 2) the air inside the fracture gets trapped preferably in the larger aperture areas since the water seeks the fine pores and the air or gas seeks the larger pores. Both processes are most likely contributing to the larger mean apertures that have been observed and both would bias the measurements towards larger apertures

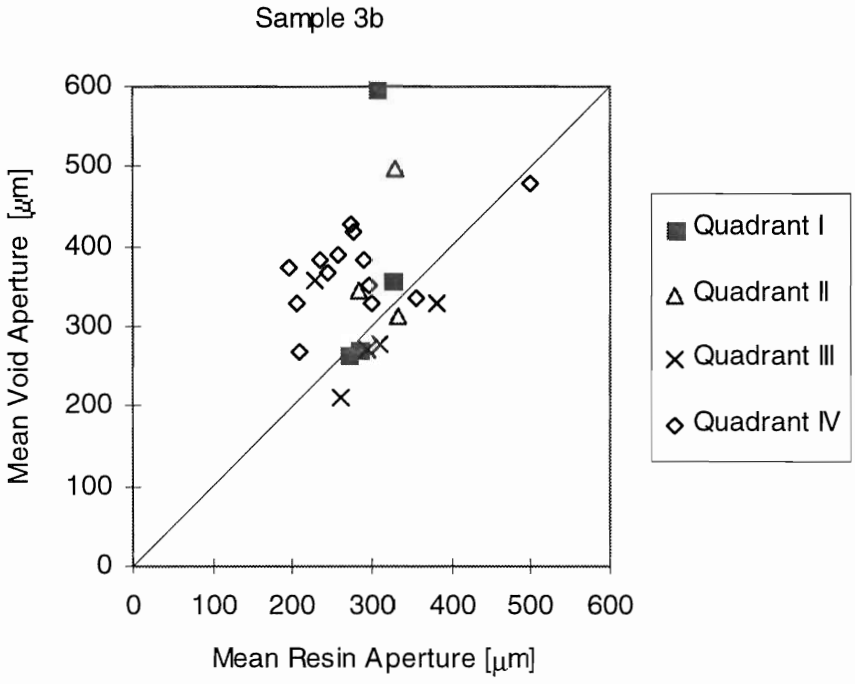

Figure 3-10 Mean aperture in void areas versus mean aperture in resin areas for measurement profiles of Sample 3b. Profiles with less than 5% void data are not included.

4 Variogram Analysis

4.1 Approach of Analysis

As discussed in this report, the fracture plane consists of open pore space and contact areas. Thus, if one samples any point in the fracture plane, one will encounter either an open part of the fracture plane, that is either resin filled, gouge filled or a void, or a part where the walls are in contact. These two fracture plane attributes can be considered as being represented by two different distributions, one for the open pore space or apertures and one for the contact areas.

If the contact areas are completely ignored and the aperture statistics are computed from the open pore space data, the aperture values that are generated using a univariate approach for any flow or transport simulation will definitely be overestimated, if they are assumed to be applicable to the entire fracture surface. In addition, the spatial continuity of the simulated aperture field over the entire fracture plane will also be overestimated. Also, the aperture or gap between the adjoining walls will vary throughout the open part of the fracture plane. However, in the contact areas, all of the measurement points are assigned a zero aperture or set to some threshold value. Thus, if all the point measurements for the contact areas are included with the aperture or resin data, a single aperture/contact area distribution will be bimodal. The bimodal nature of such a combined distribution makes it difficult to use with a univariate approach to generate the aperture field for flow and transport simulations. A geostatistical approach was used to characterize and generate the aperture field to permit the use of the combined data set without the problems that are inherent to generation using a bimodal distribution.

In the mapping strategy associated with the resin injection approach, the sampling points are not evenly distributed over the entire fracture plane. Samples are clustered along the sampling profiles, i.e., along the X and/or Y direction. By accounting both for the clustering of nearby samples and for their distances to the point being estimated, ordinary kriging handles the adverse effects of clustering much better than other methods. Therefore ordinary kriging using the whole set of data, including aperture and contact areas, was selected as the procedure for estimating the fracture pore space. No declustering of the data was performed.

The geostatistical estimations of the fracture pore space utilized the GSLIB Software fortran programs (Deutsch and Journel, 1992). The basic approach used in analyzing this set of data followed the approach taken in analyzing the resin pore space data from the degassing experiments (Gale et al., 1999) and consisted of the following steps:

1. Modeling the sample semi-variograms by using GSLIB's ***gamv2m.for*** and its sub-program ***gamv2.for***.

2. Using Excel to plot the semi-variograms, and then fitting mathematical models to the semi-variograms based on the shape of the semi-variograms and the desired accuracy. The key to successful estimation was to choose a variogram or a covariance that captured the pattern of the spatial continuity that was assumed to be representative of a complete fracture aperture profile.

3. Block kriging was completed using the GSLIB program ***okb2dm.for*** and its sub-program ***okb2d.for***, a 2-D ordinary kriging program. This program performs geostatistical estimation of the pore space using ordinary kriging for non-gridded samples. It calculates the aperture and variance values representing the aperture value of the point in the middle of each cell of a grid, or the average aperture value for each cell of the grid; i.e., point kriging or block kriging. The grid size can be easily defined within the program parameter file for both point and block kriging. The output can be plotted as a scaled colour map, showing the distribution of apertures in each cell, by using a GSLIB postscript plotting program ***cscale.for***.

4. Cross validation analyses were performed to evaluate whether or not the aperture estimates meet the desired accuracy. These calculations were performed using GSLIB program ***xvok2dm.for*** and its sub-program ***xvok2d.for***. These programs compare the estimated values at the sampled locations with the actual measured values and generate a table containing the X and Y location, the true value, the estimated value, estimation variance, and error at each sampled point. The output can be plotted as scatter plots using the GSLIB postscript program ***scatplt.for***.

Similarly, quantile/quantile or Q-Q plots, that compare the quantiles of the original data distribution and the distribution of the simulated data points provide an effective means of validating kriged results. GSLIB computes and plots the Q-Q diagrams using a postscript plotting program ***qpplt.for***.

4.2 Fracture Pore Space Variograms

The spatial continuity of apertures was determined by carrying out semivariogram analyses on both samples using the complete aperture data sets (resin + voids + contacts) for lags equal to 0.07 and 0.7 mm in the X, Y directions and 45° from the Y axis of the grid. The lag tolerance and angular tolerance used are 0.035 mm and 10.5° respectively. Semi-variograms based on a lag of 0.7 mm show similar distributions to those based on the lag of 0.07 mm, but have less consistency. Therefore models were fitted to data points representing multiples of the base lag up to 12 mm.

Figures 4.1 and 4.2 show the semi-variograms (diamond shaped data points) and fitted models (light dashed lines) in the X and Y directions of Sample 1b and 3b, respectively. For each sample, the variograms for the X and Y directions in Quadrant IV and the X and Y directions for the four combined quadrants are presented in the respective figures. For Sample 1b, all four semi-variograms appear to rise from the origin, more or less level off at distances of about 3 to 5 mm, but the value at which they level off, i.e. the initial sill, varies with direction and by quadrant. In Quadrant 1bIV, the initial leveling

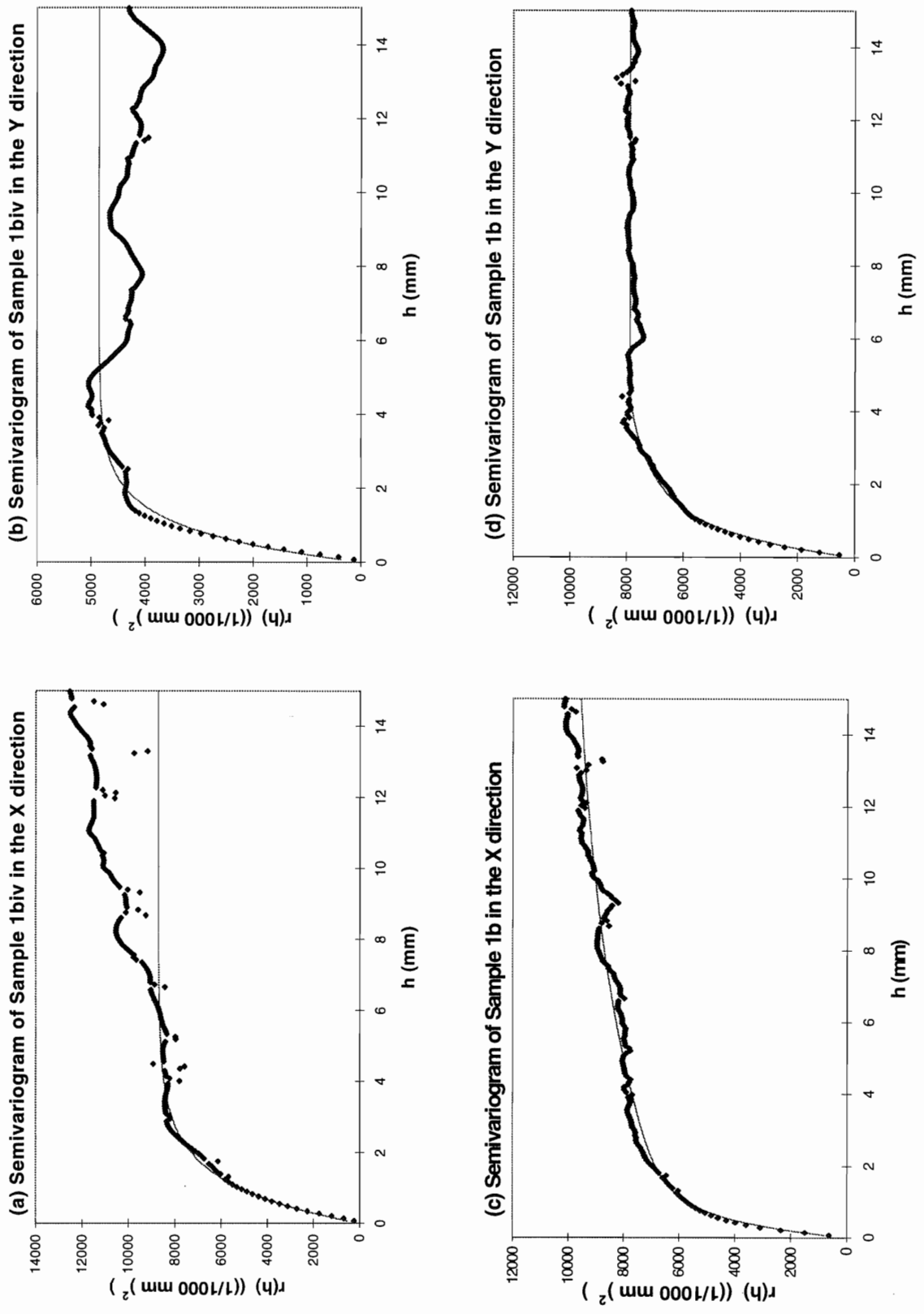

Figure 4-1 Semi-variograms for Quadrant IV and for all quadrants combined, based on the profiles in the X and Y directions, for Sample 1b.

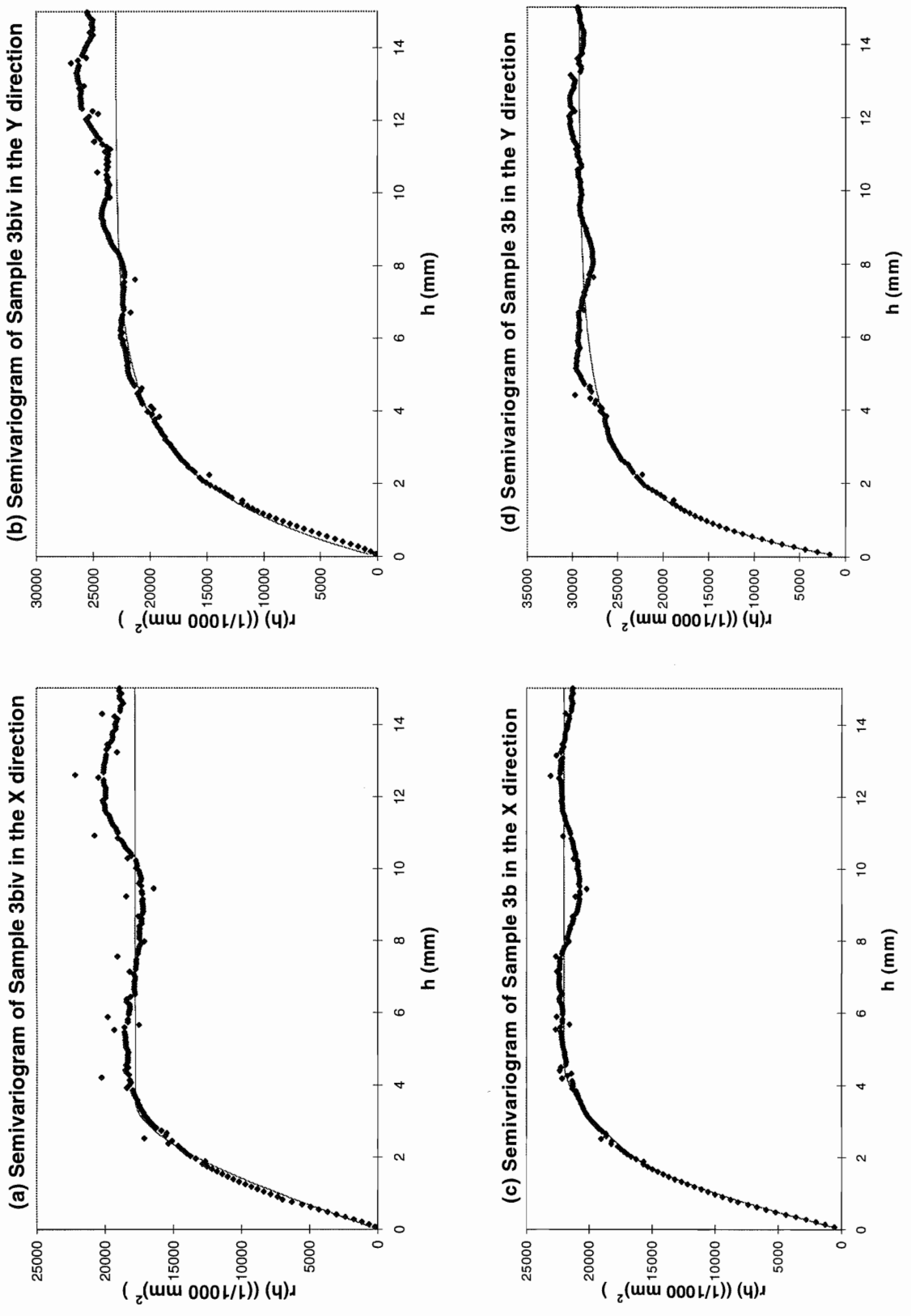

Figure 4-2 Semi-variograms for Quadrant IV and for all Quadrants combined, based on the profiles in the X and Y directions, for Sample 3b.

off point is about 8000 in the X-direction variogram and 5000 in the Y-direction. However, when all Quadrants are combined the initial levelling off points for both the X and Y directions are similar, at about 8000. Examining the supposed variation around the sill, the plot for the X direction in Quadrant IV of Sample 1b shows that at distances greater than 7 mm the differences increase, while in the plot for the Y direction in 1bIV the dips in the curve at a distance of about 6 to 8 mm and again at a distance of 12 to 14 mm suggest that there are less differences between apertures 6 to 8 and 12 to 14 mm apart than there are between apertures that are less than 5 mm apart. However, the combined data for Sample 1b, in the Y direction, show a fairly constant sill, suggesting strong continuity with distance. In the X direction, the combined data still show an increase in the difference with distance, however, the difference does not increase as rapidly as in 1bIV.

In Sample 3b (Figure 4-2), the initial leveling off point is smaller for the X direction than for the Y direction with the distance at which the levelling-off occurs being about 4 mm for the X direction in 3bIV and at about 6 mm for the Y direction in 3bIV. For the combined data sets, the curves level off at about 6 mm in both the X and Y directions. Except for the small dip in the curve for the combined data set at about 9 mm, the semi-variograms show a general increase in the difference between apertures with increasing spacing between measurement points.

In both Figures 4-1 and 4-2, the fitted models of both samples in both X and Y directions can be closely described by a nested model comprising of two exponential models. The equations used to fit the models to the semi-variograms were unnecessarily complex and have been omitted from the semi-variograms.

4.3 Kriging Estimates

Kriging estimates typically have less variability than the true value, i.e., smaller standard deviation. This reduction in variability results from the smoothing effect of estimation, and is a result of the fact that our estimates are weighted linear combinations of several sample values. Since block kriging estimates the average aperture value for each cell, defined by the size of the grid or mesh, block kriging will produce a larger smoothing effect that point kriging. As the grid size increases, the variability of the kriged result decreases. Based on modeling results reported for other samples (Gale et al., 1999), for these two samples, block kriging to map the aperture distributions was completed using a 1 mm grid size (Figures 4-3 and 4-4). The ranges of the semi-variograms and their fitted models are quite small, while the available profiles are clustered in the middle of the samples, leaving large areas unsampled. Kriging in those areas will introduce uncertainty. Kriging was therefore only completed over the areas in which profiles had been completed, hence the irregular shape of the aperture map.

In order to investigate the accuracy of the estimation, cross validations were performed. Figures 4-5 and 4-6 show the q-q and cross validation scatter plots for the measured apertures and estimated apertures based on a grid size 1.0 mm. Clearly, the cloud is distributed along the 45 degree line that goes through the origin. This indicates that the

kriging result closely predicts the true data. The q-q plots show that at very low aperture values the kriging results slightly overestimate the sample value; at high aperture values (> 1 mm), the q-q plot for sample 3b underestimates the sample apertures. However, based on the aperture frequency distribution for this sample, apertures above 1.0 mm comprises a very low percentage of the sample.

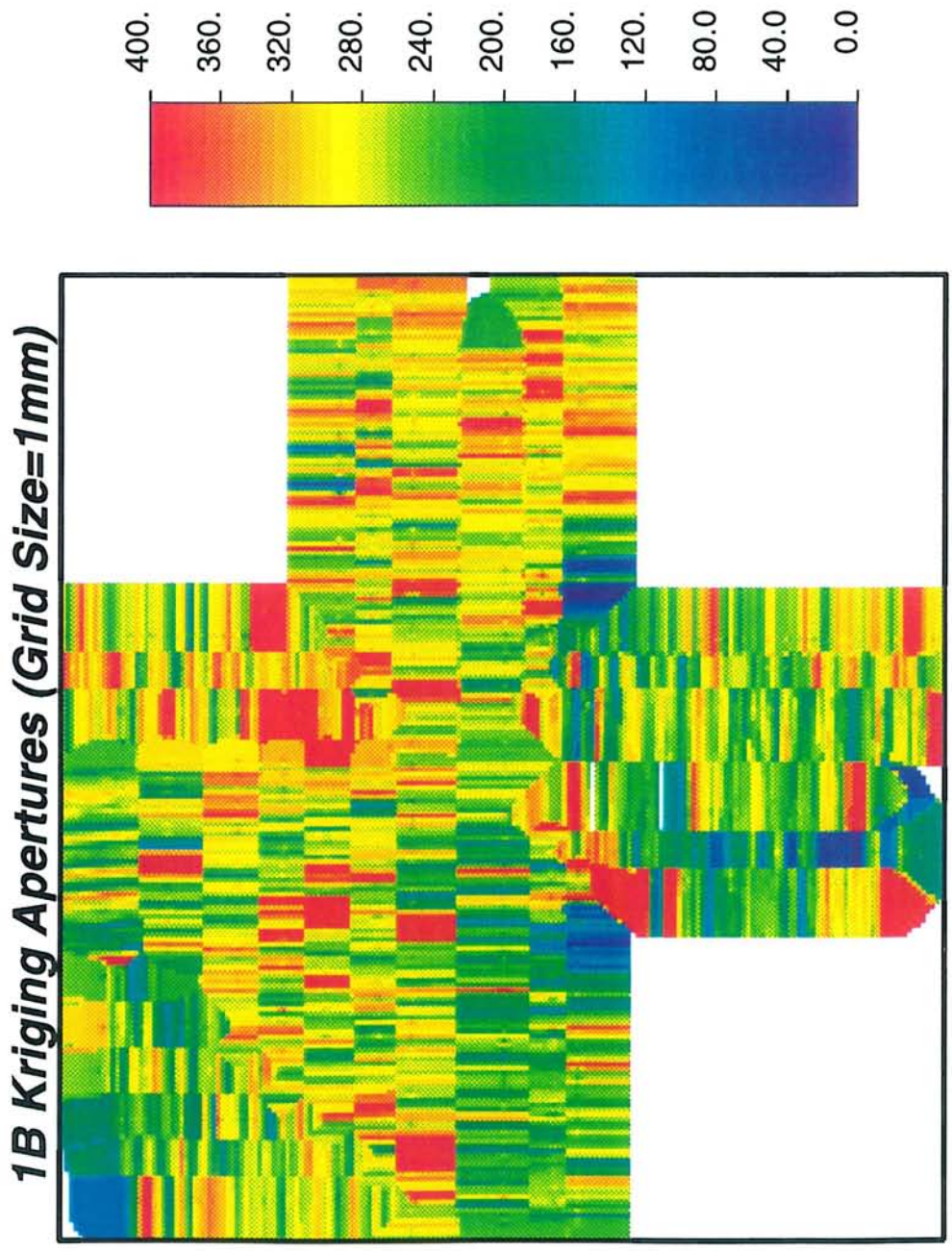

Figure 4-3 Map of apertures computed by block kriging for Sample 1b; Grid size equals 1 mm. Scale on the right hand is in micrometers.

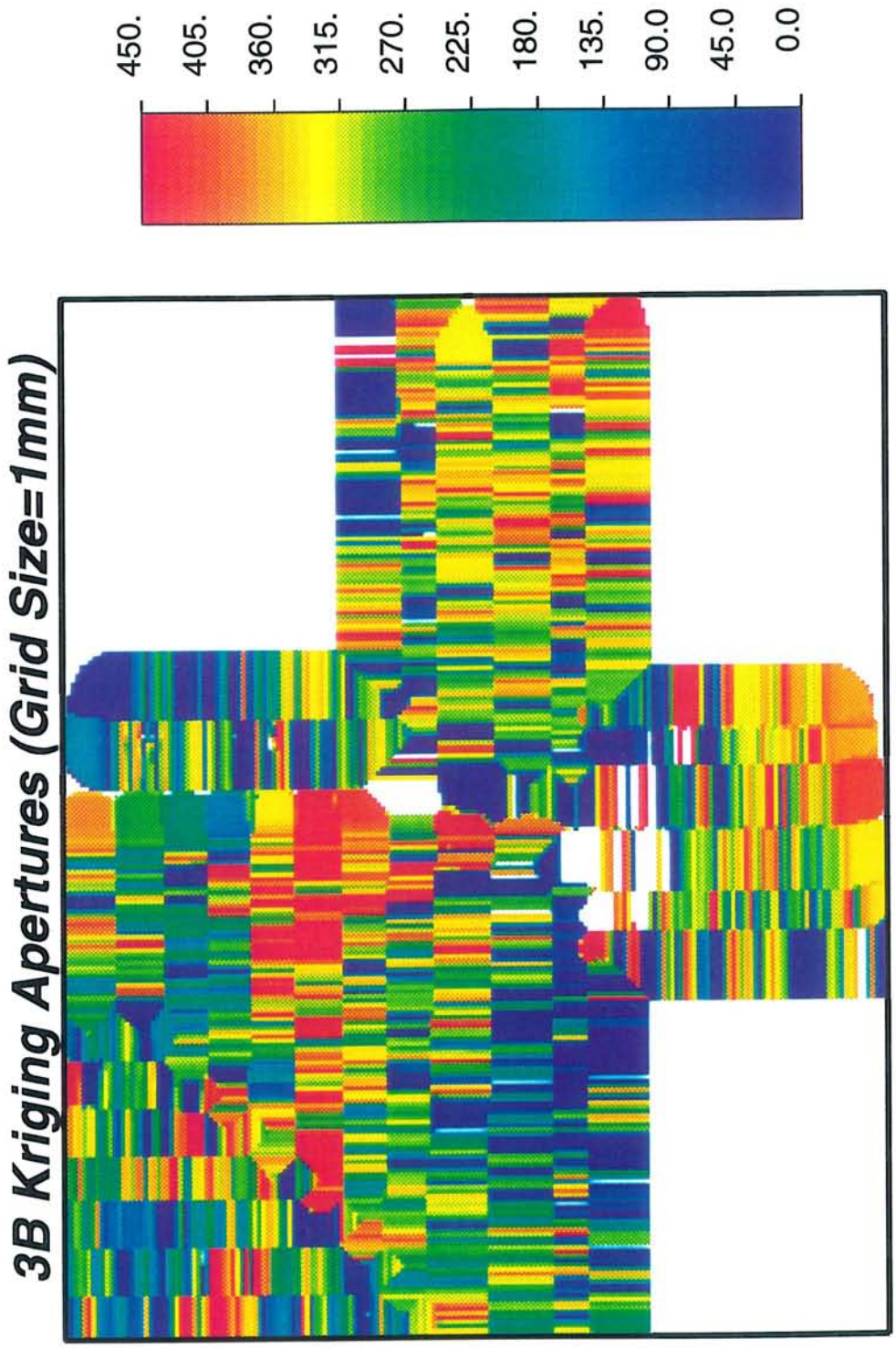

Figure 4-4 Map of apertures computed by block kriging for Sample 3b; Grid size equals 1 mm. Scale on the right hand side is in micrometers.

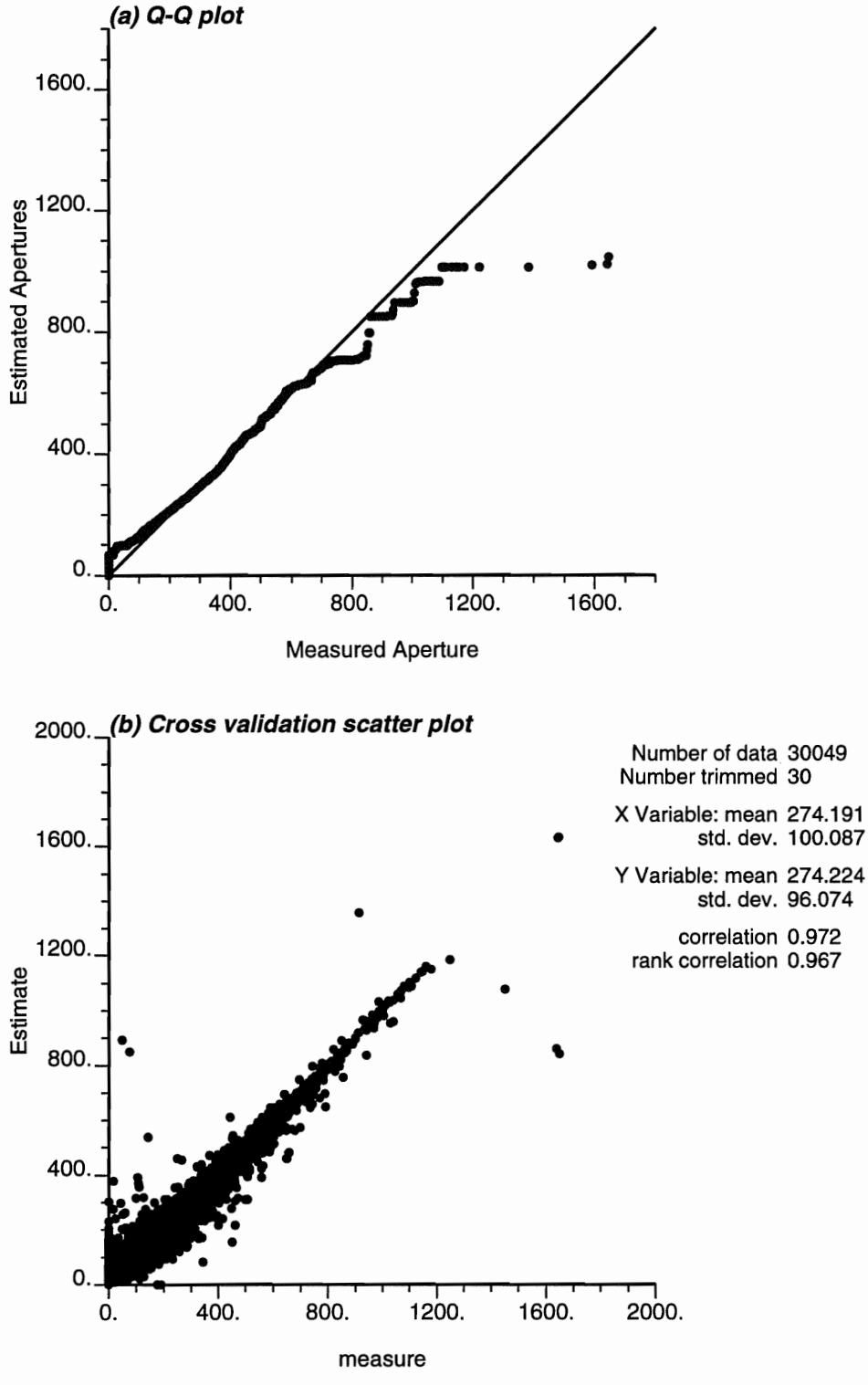

Figure 4-5 (a) Q-Q plot of the measured and estimated apertures (μm) for Sample 1b; and (b) Scatter plot of the measured values and the estimated values at the same sampling locations. Both plots show strong correlation between the measured values and the estimated values.

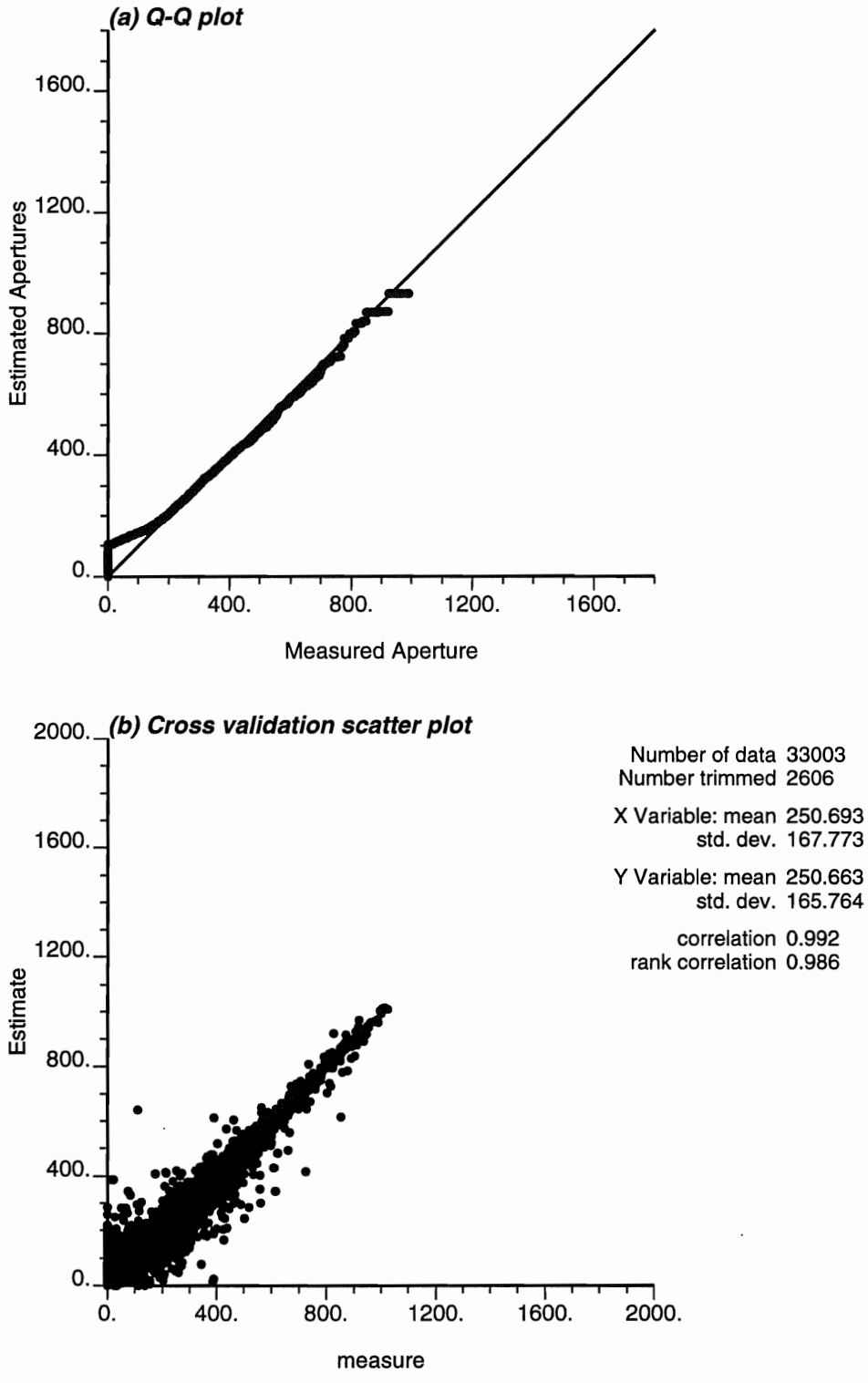

Figure 4-6 (a) Q-Q plot of the measured and estimated apertures (μm) for Sample 3b; and (b) Scatter plot of the measured values and the estimated values at he same sampling locations. Both plots show strong correlation between the measured values and the estimated values.

5 Discussion

5.1 Measurement Techniques

Both methods give the same magnitude of aperture, and similar standard deviations. Both methods have sufficient accuracy for fractures with a mean aperture larger than about 100 μm. For measurement of fractures with a smaller aperture the magnification of the measurement images must be increased to give a reasonable accuracy, which makes the measurements more time consuming. Also, tighter fractures might be difficult to impregnate with resin, resulting in more voids.

Both measurement techniques would be improved with increased colour contrast between the epoxy resin and the natural materials. Light coloured resin will be similar to light coloured minerals, such as calcite, and dark resin similar to dark minerals, such as biotite and chlorite etc. Preferably the resin should not be very transparent since the transparency make the resin appear dark in the sections and the edges of the fracture surface also appear less sharp in such cases. In previous measurements, a resin with a strongly fluorescent colour proved to function well using UV-light and a corresponding filter in the microscope. Among the colours, blue is judged to be the most preferable to obtain a good contrast. If samples of the fractures are to be studied in thin sections, the appearance of the different epoxy resin used in the injection and for the preparation process, should be clearly different in colour.

The photo-microscope technique has been the fastest technique employed in this project. The time needed for the image analysis technique is more dependent on the particular image contrast conditions of a specific fracture sample. The possibilities for automatization, and higher analysis speed, increase with good image contrast between minerals and resin.

The photo-microscope method may therefore be preferred when extensive profiles are to be measured and the fracture geometry or information is not very complex. The image analysis technique may be preferred when there is a need to attach different information to each separate data point, for example if the geometrical pattern is complex or if information about filling materials is also to be recorded. In the photo-microscope approach, the photographs and negatives provide a permanent record of the fracture section. Similarly, in the image analysis technique the digital images can be saved and used for additional geometrical or geological analysis or illustrations. This aspect of both techniques is particularly valuable in cases where the rock samples are destroyed after measurement, for example due to cutting of very thin sample slabs.

5.2 Measurement Results

The results gained in this study concerning aperture spatial distribution may be compared to what has been found in previous studies Figure 5-1 shows a compilation of results from different fracture samples measured with different techniques (Hakami, 1995). In the diagram the spatial continuity of the aperture distribution is related to the variation. The coefficient of variation is the ratio between the standard deviation of the total data (also including contacts) and the mean. The (practical) range is the lag distance at which the semi-variogram value reaches 95% of the sill. It should be noted that the data in the figure are compiled and presented together although they represent results from different geological types of fractures, and that the data have not been collected under similar stress conditions.

In the diagram the two results from this study are also inserted for comparison. The results from Sample 1b and 3b both fall well within the range of values found in the earlier investigations.

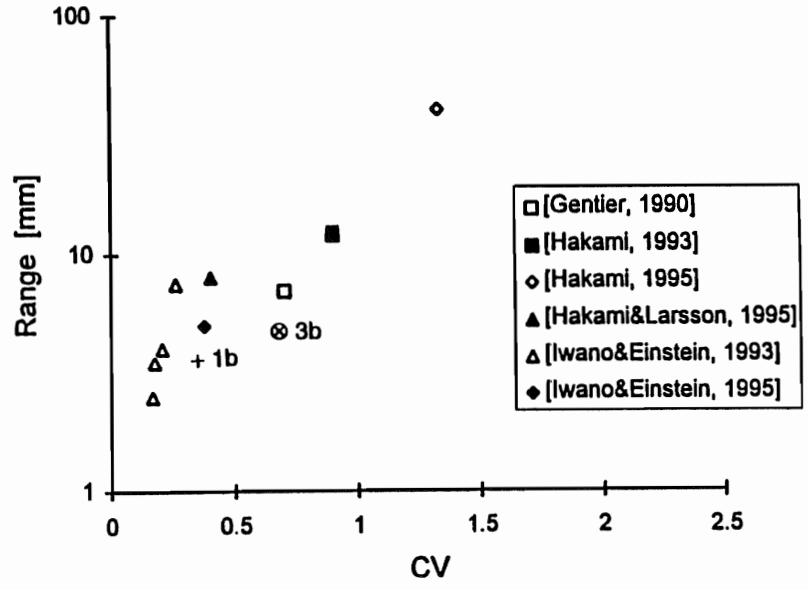

Figure 5-1 Compilation of fracture aperture data: Range (correlation length) versus Coefficient of variation (CV). Both range and CV calculated for all data, inculding contacts; from (Hakami, 1995). The results from samples 1b and 3b are marked in the diagram for comparison.

5.3 Spacing of Measurement Points

The sensitivity analysis performed in this study using the image analysis system, demonstrates that the amount of data generated can be decreased by using a greater distance between measurement points, along each profile, without affecting the aperture statistics. The impact that more widely spaced measurement points would have on the constructed semi-variograms has, however, not been investigated.

To be able to compare measured apertures with interpreted apertures in flow experiments, and validate the flow and transport conceptual models, a map of the aperture distribution is often desirable. In order to make a kriged map, with an acceptable accuracy for points between measurement profiles, the profiles have to be spaced no more than the range (correlation distance). This spacing may be achieved in laboratory experiments where the fracture sample area is limited.

However, since the range of fracture aperture distributions has been generally found to be short (maximum centimeters) it is not possible, of technical and economical reasons, to get sufficient measurement profiles to make a kriged map over the whole fracture area involved in a field experiment, such as TRUE. Nevertheless, results from single measurement profiles, or profiles with large spacing, will be invaluable in constructing realistic models of the aperture distribution at a specific site. Such aperture distribution models may then be used to stochastically generate aperture distributions for simulations of flow and transport at the site.

6 Conclusions

6.1 Aperture Distribution at the Pilot Resin Site

Samples were taken from two different fractures, Sample 1b and Sample 3b, both located at the Pilot Resin Site at Äspö HRL. The two collected samples are taken from fractures with different orientation having different character in terms of geological history and hydromechanical properties. Both fractures are representative of the fractures observed at the Äspö HRL.

Mean aperture of Sample 1b is about 281 μm. The standard deviation of the aperture is about 37% of the mean aperture. Sample 1b contains little contact area, only about 1% of the whole sample.

Mean aperture of Sample 3b is about 295 μm (contact areas and void areas not included). The standard deviation of the aperture is about 39% of the mean aperture. Sample 3b contains about 22% contact area and about 20 % void area. Therefore, if the mean aperture is calculated instead for all data, including contacts and voids, it becomes smaller, namely 239 μm.

To describe the fracture pore space geometry one must consider not only the probability distribution of the apertures but also the contact areas and the spatial structure of apertures and contacts within the fracture. If the contact areas are ignored in the generation of an aperture field for flow and transport simulations, the flow capacity and hence transport capacity of the fracture will be over-estimated.

The spatial pattern of apertures and contacts can be analyzed with geostatistical methods such as semi-variograms. The experimental variograms can be described by the parameters of fitted variogram models. In this study, the practical range of the semi-variograms for Sample 1b was determined to about 3.5 mm and 5 mm for Sample 3b. No clear anisotropy was found in the aperture distributions of these two samples.

A variogram model together with a probability distribution model may be used in stochastic simulation of the aperture field of a fracture. Mapping the aperture field using kriging based on measurements of apertures and contacts, provides a realistic simulation of the spatial structure, if the measurements are sufficiently densely spaced. Also less dense measurement data will be invaluable in constructing the conceptual models of the pore space geometry needed in flow and transport modeling.

6.2 Recommendations for Future Work

A number of recommendations have been presented in this report. It is clear, that both of the aperture mapping techniques provide similar results with a similar level of precision for the scales being used. It is obvious that the image analysis approach is more flexible in terms of adjusting the image scale to map finer details in the fracture pore space. By contrast, the photo-microscope approach can be completed with less equipment and faster than the image analysis approach. The decision as to which approach to use depends in part on the goal of the aperture measurement exercise. Clearly, the addition of additives to the resins, that facilitate the automation of the image analysis approach, will significantly increase the speed at which the samples are processed and analyzed. Hence, a major thrust of future work will be to identify dyes or additives that do not interfere with the resin bonding process, but at the same time permit the automation of the image analysis approach.

References

Deutsch, C.V. and Journel, A.G., 1992. GSLIB, Geostatistical Software Library and User's Guide. Oxford University Press, 340 pp.

Birgersson, L., Gale, J. and Hakami E., 1999. First TRUE Stage - Pilot Resin Injection Experiment - Final Report, Part 1. SKB Äspö HRL PR 99-xx (in prep).

Gale, J., 1999. Impact of flow geometry, flow regime, two-phase flow and degassing on the transmissivity of rough fractures. SKB (in prep.).

Hakami, E., 1995. Aperture Distribution of Rock Fractures, Doctoral Thesis, Royal Institute of Technology, Division of Engineering Geology, Stockholm, ISBN 91-7170-835-9.

Laaksoharju, M. (ed.), 1995. Sulphate reduction in the Äspö HRL tunnel. SKB Technical Report. TR 95-25. ISSN 0284-3757.

Winberg, A. (ed.), 1999. Tracer Retention Undersstanding Experiments - First TRUE Stage Final Report. SKB Technical Report TR 99-xx (in prep.).